MODELING AND SIMULATION OF OIL LEAKAGE IN RADIAL LIP SEALS

A THESIS SUBMITTED TO
THE GRADUATE SCHOOL OF NATURAL AND APPLIED SCIENCES
OF
MIDDLE EAST TECHNICAL UNIVERSITY

BY

MELTEM YILDIZ

IN PARTIAL FULFILLMENT OF THE REQUIREMENTS
FOR
THE DEGREE OF MASTER OF SCIENCE
IN
MECHANICAL ENGINEERING

APRIL 2010

Approval of the thesis:

MODELING AND SIMULATION OF OIL LEAKAGE IN RADIAL LIP SEALS

submitted by **MELTEM YILDIZ** in partial fulfillment of the requirements for the degree of **Master of Science in Mechanical Engineering Department, Middle East Technical University** by,

Prof. Dr. Canan Özgen _____
Dean, Graduate School of **Natural and Applied Sciences**

Prof. Dr. Suha Oral _____
Head of Department, **Mechanical Engineering**

Prof. Dr. Metin Akkök _____
Supervisor, **Mechanical Engineering Dept., METU**

Examining Committee Members:

Prof. Dr. Haluk Aksel _____
Mechanical Engineering Dept., METU

Prof. Dr. Metin Akkök _____
Mechanical Engineering Dept., METU

Prof. Dr. Nafiz Alemdaroğlu _____
Aerospace Engineering Dept., METU

Prof. Dr. Kahraman Albayrak _____
Mechanical Engineering Dept., METU

Prof. Dr. Suat Kadıoğlu _____
Mechanical Engineering Dept., METU

Date: _____

I hereby declare that all information in this document has been obtained and presented in accordance with academic rules and ethical conduct. I also declare that, as required by these rules and conduct, I have fully cited and referenced all material and results that are not original to this work.

Name, Last name: Meltem Yıldız

Signature :

ABSTRACT

MODELING AND SIMULATION OF OIL LEAKAGE IN RADIAL LIP SEALS

Yıldız, Meltem

M.Sc., Mechanical Engineering Department
Supervisor: Prof. Dr. Metin Akkök

April 2010, 92 pages

Radial lip seals are used to prevent leakage between machine elements in many industrial applications. During operation, fluid film between seal lip and shaft surface generates a pressure distribution on the lip which is elastically deformed due to hydrodynamic pressure. Surface roughness parameters in terms of moments of height profile distribution (rms roughness, skewness and kurtosis) affect the rate of oil leakage.

A computer program is developed for elastohydrodynamic analysis of radial lip seals. Both the fluid mechanics of the lubricating film and the elastic deformation of the lip are taken into consideration to determine the hydrodynamic pressure distribution and the oil flow through the seal lip. The effect of shaft surface roughness on hydrodynamic analysis is taken into account by using average Reynolds equation with flow factors. For non-Gaussian surfaces, the modified flow factors are used to investigate the effects of skewness and kurtosis on the oil leakage. Numerical tests are performed for different skewness, kurtosis and initial seal tightness values. Results show that when a seal is

mounted with a high initial tightness, the hydrodynamic pressure developed is not enough to deform the lip to form a fluid film between the shaft and the seal lip. It is observed that for the same rms roughness and skewness, the side flow rate increases as the kurtosis value increases. However, for the same rms roughness and kurtosis values, the side flow rate decreases for all skewness values.

Keywords: Radial Lip Seals, Oil leakage, Elastohydrodynamic Lubrication, Lip Deformation, Surface Roughness, non-Gausssian Surfaces.

ÖZ

RADYAL DUDAKLI SIZDIRMAZLIK ELEMANLARINDA YAĞ KAÇAĞININ MODELLENMESİ VE SİMULASYONU

Yıldız, Meltem

Yüksek Lisans, Makine Mühendisliği Bölümü
Tez Yöneticisi: Prof. Dr. Metin Akkök

Nisan 2010, 92 sayfa

Radyal dudaklı sızdırmazlık elemanları, makine elemanları arasında sızıntıyı önlemek amacıyla farklı endüstriyel uygulamalarda kullanılmaktadır. Çalışma sırasında, sızdırmazlık elemanı dudağı ile dönen mil arasındaki açıklıkta oluşan akışkan filmindeki hidrodinamik basınç ile dudak yüzey şekli değişmektedir. Yüzey profil yükseklik dağılımının momentlerine göre tanımlanan yüzey pürüzlülüğü parametreleri (rms pürüzlülük, simetriklik, sivrilik) yağ kaçağı miktarını etkilemektedir.

Radyal dudaklı sızdırmazlık elemanlarının elastohidrodinamik analizi için bir bilgisayar programı geliştirilmiştir. Yağ kaçağı ve hidrodinamik basınç dağılımı analizinde, yağ filminin akışkan mekaniği ve sızdırmazlık elemanı dudağının elastik şekil değişikliği göz önünde bulundurulmuştur. Mil yüzeyinin pürüzlülüğünün etkisi, akış katsayıları ile ortalama Reynolds denklemi çözülerek, hidrodinamik analizde dikkate alınmıştır. Gauss dağılımı olmayan yüzeyler için değiştirilen akış katsayıları, simetriklik ve sivrilik değerlerinin yağ kaçağı üzerine etkisini incelemek amacıyla kullanılmıştır. Yüzey profil

yükseklik dağılımının farklı simetriklik ve sivrilik değerleri ile sızdırmazlık elemanının ilk sıkılık değeri için sayısal simülasyon uygulanmıştır. Sonuçlar, mile fazla sıkı geçirilen bir sızdırmazlık elemanında oluşan hidrodinamik basıncın dudakta şekil değişikliğine yol açacak ve mil ile dudak arasında film tabakası oluşturacak kadar yeterli olmadığını göstermektedir. Aynı rms pürüzlülük ve simetriklik değerleri için yağ kaçak miktarının sivrilik değeri ile arttığı gözlenmiştir. Ancak, aynı rms pürüzlülük ve sivrilik değerleri için yağ kaçak miktarı yüzeyin simetriklik değeri ile azalmaktadır.

Anahtar Kelimeler: Radyal Dudaklı Sızdırmazlık Elemanları, Yağ Kaçağı, Elastohidrodinamik Yağlama, Dudak Şekil Değişikliği, Yüzey Pürüzlülüğü, Gauss Dağılımı Olmayan Yüzeyler.

To My Mother

ACKNOWLEDGEMENTS

The author would like to express her deep gratitude to her supervisor Prof. Dr. Metin Akkök, who made this work happen, for his guidance, supervision and encouragement.

And I am deeply indebt to my family for their never-ending love and spiritual support at critical and opportune times.

I am grateful to my friends for the care with which they helped me prepare this thesis; and for conversations that clarified my thinking on this and other matters. Their friendship and professional collaboration meant a great deal to me.

TABLE OF CONTENTS

LIST OF TABLES

LIST OF FIGURES

NOMENCLATURE

A : Deformation parameter, $\frac{6\mu UB^2}{E_r\sigma^3}$

B : width of slider bearing along the sliding direction

c, d : Element boundaries from centre

$\bar{c}$, $\bar{d}$: Non-dimensional element boundaries from centre

E_r : Reduced Young's modulus, $1/\left\{\frac{1}{\pi}\left(\frac{1-v_1^2}{E_1}+\frac{1-v_2^2}{E_2}\right)\right\}$

h : Film thickness

H : Non-dimensional film thickness, $\frac{h}{\sigma}$

h_m : Minimum film thickness

h_T : Local film thickness

I : Influence coefficient matrix

K : Kurtosis

L : length of slider bearing in the transverse direction

M, N : Number of nodes

m : Inclination of the bearing

p : Pressure distribution

P : Non-dimensional pressure, $\frac{p}{6\mu UB/\sigma^2}$

q : Total side flow

RF : Relaxation Factor

rs : Summation of absolute residual

xs : Summation of absolute pressure

Q : Non-dimensional side flow, $\frac{q}{\sigma BU/2}$

S_k : Normalized skewness of the heights

U : Velocity of slider

v_1, v_2 : Poisons ratios of the materials

w : Load support

W : Non-dimensional load support, $\frac{wh_m^{\ 2}}{6\mu ULB^2}$

ws : Absolute weighted residual

μ : Absolute viscosity

ϕ_x : Pressure flow factor in x direction

ϕ_y : Pressure flow factor in y direction

δ_1, δ_2 : Random roughness amplitudes

σ_1, σ_2 : Zero mean and standard deviations

γ : Mean ellipticity ratio (Peklenik number)

$\phi(z)$: Surface profile height distribution

Φ_s : The shear flow factor

σ : composite rms roughness

$\hat{\phi}$: Pressure flow factor for non-Gaussian roughness

ϕ' : Pressure flow factor for Gaussian roughness

δ : Total deflection

$\bar{\delta}$: Non-dimensional deflection, $\frac{\delta}{\sigma}$

λ : undulation wave length

CHAPTER 1

INTRODUCTION

Radial lip seals are used to prevent leakage between dynamic or static machine elements in many industrial applications at a wide range of temperatures and pressures. The function of a seal is to separate pressurized fluids where, for instance, a moving shaft passes through a machine housing or passes from one part of the machine to another. It may also serve to prevent entry of foreign particles into an operating medium or the loss of lubricant from bearings and transmissions. Although a full contact between the seal and the shaft surface provides perfect sealing, it is not preferred because of high friction and wear. To reduce friction and wear, the gap between the seal and the shaft is full of lubricant film but it may cause to leakage of the lubricant through the seal. Well designed radial lip seals produce an acceptably low level of leakage with a thin fluid film between the shaft and the seal to function effectively for low friction and low wear.

1.1 Basic Construction of Radial Lip Seals

In industry a large number of seals are used to help to solve the problems presented by fluid sealing needs. Many individual internal and external factors, as well as interactions between them, affect the rate of seal leakage. Some design features or treatments enhance reliability but contribute to some marginal increase in leakage.

Baart, Lugt, Prakash [1] presented a review of the lubrication, sealing and pumping mechanisms in oil and grease lubricated radial lip seals. The seal is mounted on a shaft

with an interference fit. A garter spring is used to build up preload between the seal lip and the shaft throughout the seal life. The lip contacts with the shaft at two angles: the air-side angle α and the lubricant side angle β as seen in Figure 1.1. As an experienced know-how, seals are designed with a smaller angle at the air-side than the lubricant side to keep the lubricant inside the system. The functioning of the lip comes from its asymmetrical geometry.

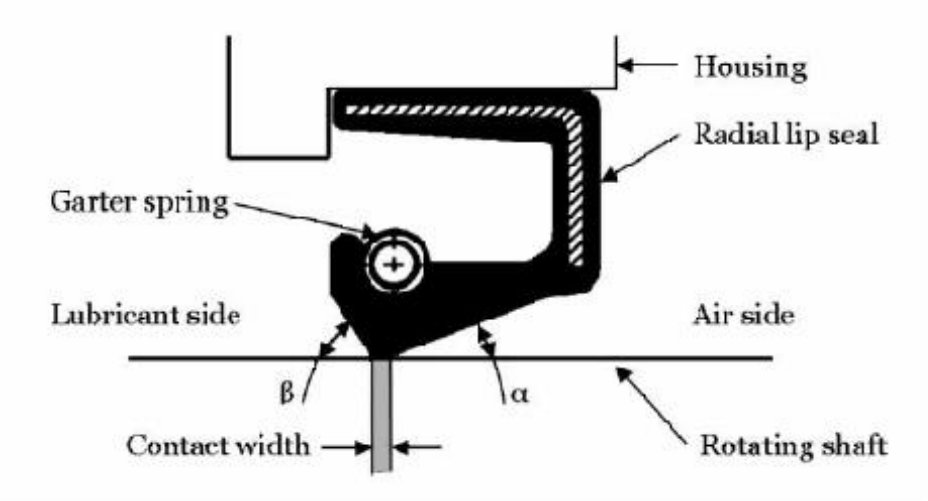

Figure 1.1 Arrangement of a radial lip seal on a rotating shaft [1]

Seals are made of viscoelastic materials such as elastomers. A reliable seal design should provide a restricted flow of fluid in a prescribed service environment. The reliability of a seal design is determined by the ability of the seal to restrict the flow. In order to estimate the reliability of a seal design, it is required to define the design parameters and the operating conditions. Seals have not universal design to use all applications. Design aspects of radial seals are reviewed by Johnston [2].

Standards for simple seal are defined by most seal manufacturers for most important parameters such as lip height, flex section thickness, radial load and spring characteristics for a particular shaft diameter (Figure 1.2).

Typically α is of the order of 25-30° and β about 40-45° on a seal. The rotational movement of the lip is amount to about 10° when seal is mounted on the shaft. H_L ranges from about 2 to 5 mm, and the size is proportional to the shaft diameter. Larger lip size is used to increase contact region between elastomer and shaft and to provide more space for larger and stiffer springs.

The thickness t is normally described as the minimum value at the metal case or insert end, of the order of 40 per cent of the lip height. Seals are designed with large t values for high pressure applications and with low t values for flexibility in large shaft deflections.

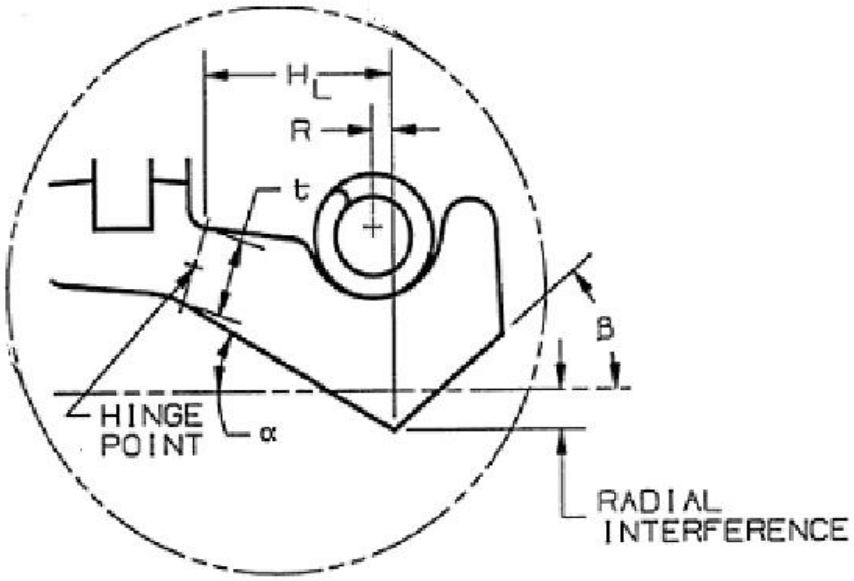

Figure 1.2 Basic construction of a radial seal [2]

The pressure distribution in the elastomer contact edge is asymmetrical to provide the pumping action as shown in Figure 1.3.

As mentioned previously, the pressure distribution in the contact area is expected to be asymmetrical to provide the pumping action. The maximum pressure distribution is skewed to the oil side edge by putting the spring on the air side of the contact.

R value is defined as the axial distance between the hinge point of the lip and the contact edge and taken as about 10 per cent of the length of the lip. Larger value of R may cause the lip to deflect, and also reduces the influence of the spring load on the contact pressure distribution.

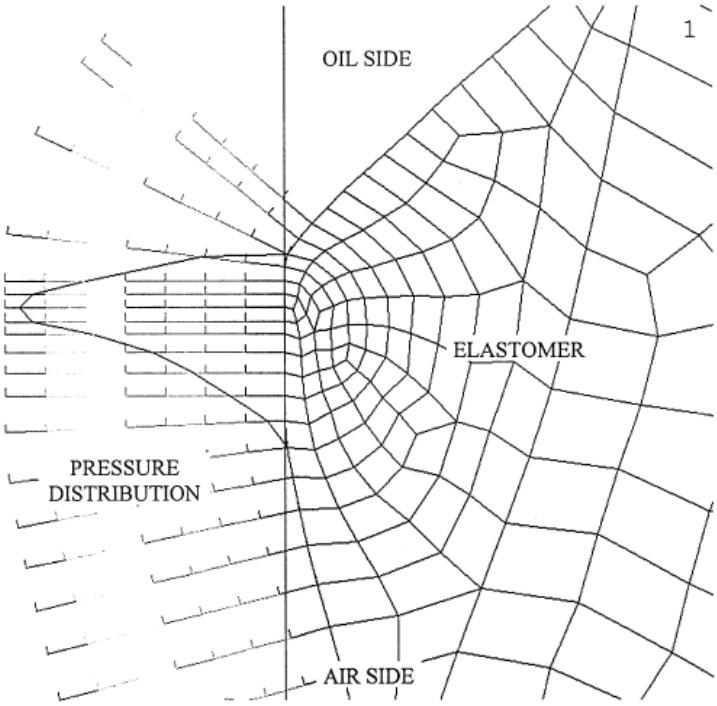

Figure 1.3 Pressure distribution on the shaft in the contact area of a lip seal [2]

1.2 Sealing Mechanisms

In literature, the performance of radial lip seals can be explained by three mechanisms: the sealing, lubrication, and pumping mechanism. The sealing mechanism provides both static and dynamic sealing and helps to keep the lubricant inside and contamination outside the system. The lubrication mechanism is explained by the fluid mechanism of the lubricant. The lip is separated from the shaft surface by a thin lubricant film between the lip and the rotating shaft reducing friction and wear. Pumping of the lubricant from the air side back to the lubricant side is explained by the pumping mechanism.

Five of seal properties which are observed during experiments are presented to identify the lubrication, sealing, and pumping mechanism:

(a) there may exist a lubricating film under the lip;
(b) successful seals pump lubricant from airside to the lubricant side;
(c) the microgeometry of the lip surface has an important role;
(d) the macrogeometry of the lip plays an role;
(e) seal life depends on lip temperature.

Sealing is provided by the surface tension of the hydrodynamic oil film between the seal lip and shaft. Optimum oil film thickness is of the order 0.25 μm. Any greater film thickness tends to promote leakage; any less film thickness increases friction and wear. The continued presence of a consistent oil film is thus most important in providing lubrication for the seal.

1.3 Roughness and Microgeometry

The microgeometry of the lip identifies surface roughness of the lip. The seal surface in dynamic conditions is characterized by the resulting roughness pattern. Axially extended undulations or irregular microasperities may be observed over the contact surface as seen in Figure 1.4. The development of this roughness pattern depends very much on the choice of seal material.

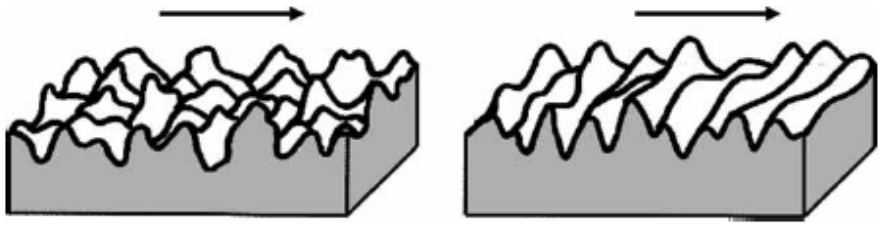

Figure 1.4 Roughness geometries: irregular microasperities (left) and axially extended undulations (right). The arrow indicates the sliding direction.

An extensive theoretical and experimental research can be found in literature. However, it is still not fully explained how these seals function. In this study, the pressure distribution under the lip, lip seal deformation and surface roughness effects on seal lip performance is studied in detail.

1.4 Characteristics of Rough Surfaces

The surface parameters are usually expressed as the center line average roughness (Ra) or the root mean square (RMS) roughness (σ). However, those parameters neglect the surface descriptions. Though surface profiles may have the same Ra or σ, they could have different height profile distributions.

The probability of locating a point at a height z for a surface height distribution is given by the probability density function $\phi(z)$ in terms of moments of the function about the mean, referred to as central moments. The first moment about the mean m line gives zero while the second moment is the variance σ^2, the square of the standard deviation,

$$\sigma^2 = \int_{-\infty}^{\infty} z^2 \phi(z) dz$$

The third standardized moment is the skewness, which represents asymmetric spread of the height distribution and is given by

$$Sk = \frac{1}{\sigma^3} \int_{-\infty}^{\infty} z^3 \phi(z) dz$$

A Gaussian surface with an equal number of peaks and valleys at certain heights has zero skewness. Height profiles with small peaks and deep valleys have negative skewness whereas profiles with small valleys or high peaks have positive skewness.

The fourth standardized moment is termed kurtosis, which represents the peakedness of the distribution and is given by

$$K = \frac{1}{\sigma^4} \int_{-\infty}^{\infty} z^4 \phi(z) dz$$

The kurtosis describes the degree of pointedness or bluntness of height profile and measures the sharpness of symmetric distribution. The kurtosis values are always positive. Gaussian height distribution has a kurtosis of 3. If the distribution has relatively small peaks and low valleys, kurtosis value is less than 3. If the distribution has more high peaks and low valleys, kurtosis value measures more than 3.

Thus, skewness (Sk) and kurtosis (K) of a rough surface give information about the shape of asperities distribution and used to represent a more exact surface profile.

CHAPTER 2

LITERATURE SURVEY ON OIL LEAKAGE IN RADIAL LIP SEALS

The purpose of this chapter is to review the literature about elastohydrodynamic lubrication to understand the behavior of seals. Related literature is given for roughness effect on oil leakage and elastohydrodynamic analysis in lip seals separately. Finally the scope of the thesis is presented.

2.1 The Effects of Roughness Orientation on Oil Leakage in Radial Lip Seals

In practice, the surface finish of the shaft at the nominal contact strip must be of a high order. Scratches or other surface imperfections can result in local thickening and breakdown of the oil film, and consequent leakage from the seal. Surface roughness can result in peaks extending through the surface of the extremely thin oil film to make dry contact with the seal lip itself, and consequently produce high wear. On the other hand, too smooth a shaft finish may inhibit wetting and retention of the oil film on the shaft.

The various equations for elastohydrodynamic film thickness assume perfect surfaces or a minimum thickness which is large compared with the vertical scale of surface roughness. However, many engineering systems operate with an estimated minimum film thickness where surface topography may play an important role. Therefore, the surface roughness should be included in any proper estimate of the surface separation, if any.

The importance of roughness effects on hydrodynamic force has gained considerable attention in the tribology literature.

Patir and Cheng [3] derived the Reynolds equation for the average pressure by using flow factors to account for the effect of roughness on the pressure. These factors were obtained through numerical flow simulation of a rough surface having a Gaussian distribution which can simulate different types of asperity geometry. Some of the asperity shapes are given in the paper. Their shape is defined by a parameter, which is a measure of the surface pattern or asperity aspect ratio. Patterns are purely transverse, isotropic or longitudinal to the entrainment flow. Using these various roughness patterns, the average flow Reynolds equation, the bulk deformation elasticity equation, the force-compliance relationship for the asperity contacts, and the temperature equation for heat generation solve simultaneously and the results are given in the study.

An average Reynolds equation capable of predicting the effects of roughness induced inter-asperity cavitation is introduced by Salant and Harp [4]. Salant and Harp has extended the flow factor method to cavitating flows. Cavitation is described by the Jakobsson-Floberg-Olsson (JFO) model in this study. Numerical experiments are applied to calculate the modified flow factors which depend on the local surface separation, surface statistics, and cavitation number. The model is extended into a general Reynolds equation to predict the combined effects of inter-asperity cavitation and macroscopic cavitation. Both the Patir and Cheng method and the present model are verified in numerical experiments.

The studies described above are limited to asperities with the major axis parallel or perpendicular to the direction of motion. In the lip seal, the asperity orientation varies continuously over the sealing zone, and that varying pattern is crucial to the load carrying capacity and pumping mechanisms for a successful seal. A method of

transforming the parallel and perpendicular flow factors to those for any arbitrary orientation was developed by Lo [5].
The method is capable of dealing with the change in roughness orientation and introduces a modified Reynolds equation with flow factors that are functions of an initial parallel or perpendicular configuration that has been transformed to an orientation angle.

In another study, Salant and Rocke [6] analyze the flow of the lubricating film on a rotary lip seal by solving the Reynolds equation with flow factors. The behavior of such a flow field is affected by the asperities on the lip surface. Since previous analyses included those asperities significantly, they required very large computation times. Salant and Rocke method is required much less computation times because the asperities are treated statistically. Cavitations and asperity orientation are considered in the computation of the flow factors. Results of the analysis present the effects of the operating parameters of the seal and the characteristics of the asperities on seal characteristics, the pumping rate and the load support.

Letalleur, Plouraboue´ and Prat [7] presented an average flow model of rough and sinusoidal surfaces lubrication. Simple unidirectional sinusoidal wavy surfaces are chosen to investigate lubricant film flow between two parallel surfaces in sliding motion. Flow factors are derived to describe the roughness impact on the macroscopic flow and shear. Smooth-rough stationary case and rough-rough unstationary case are distinguished. An average description of the surfaces roughness impact is presented.

Letalleur, Plouraboue´ and Prat [8] developed an average flow model which provides an average description of the surfaces roughness impact. The effects of lubricant film flow, pressurized and sheared between two parallel sinusoidal wavy surfaces in sliding motion are studied analytically. Two case studies are studied for stationary and time dependent local aperture configurations. Flow factors for sinusoidal surfaces are generated in this

paper. Special attention is paid to the flow factor analytical behavior when surfaces are near contact.

In another study, the influence of the roughness model on the thermo elastohydrodynamic performances of lip seals is studied by Hajjam and Bonneau [9]. In this study, three mathematical roughness models of the lip surface are developed by TEHD analysis and the influence of the surface roughness on features such as power loss, average and minimum thickness of the lubricant, reverse pumping, the average temperature is analyzed. It is considered that the lip seal is perfectly elastic, the rotating shaft perfectly smooth and the seal perfectly centered. The results showed that the choice of the mathematical model to represent the surface irregularities of the lip strongly influences the ThermoElasoHydroDynamics (TEHD) characteristic of the lip seal and particularly the reverse pumping rate.

In recent studies, flow factors for non-Gaussian roughness are generated by Morales-Espejel [10]. A simple analytical transformation is derived to obtain the pressure flow factors by extending the stochastic averaging techniques for lubricated rough surface contacts. The method is compared with results from numerical solutions available in the literature and it shows good agreement.

In another paper, Peeken [11] focus on the numerical determination of Patir and Cheng's flow factors for general roughness patterns. Surface roughness and flow simulation is improved by treating roughness as two-dimensional random process. The methods described in the paper are applied to special choices of correlation and distribution to make direct comparisons with published results available. Flow factor results are computed for 10 simulations and compared with the flow factors of Elrod, Tripp and Patir, Cheng.

2.2 Elastohydrodynamic Lubrication Analysis In Lip Seals

In most of the studies, lip-seal deformation was presented as an axisymmetric model. 3D elastic approaches on the radial lip seals are presented by Maoui, Hajjam, Bonneau [12].

The aim of this study is to determine the effects of the 3D elastic aspect of the lip on the elastohydrodynamic characteristics of the lip seals. The numerical simulation of comparative elastohydrodynamic lubrication between axisymmetrical and 3D elastic approaches on the radial lip seals is given by the solution of Reynolds Equation with the finite volume method. The results showed that the 3D effect of the elastic aspect of the seal lip is determined as a significant effect on the pumping rate values.

A numerical model which presents the behavior of the rotary lip seal with an ingested meniscus under normal operating conditions is developed by Salant [13]. The observations which are used to construct the model are given in the paper. One of them is that the pressure driven flow and reverse pumping flow are the two flows occur within the sealing zone. The elastohydrodynamic analysis is performed using the iterative computation procedure which includes initial film thickness distribution assumption, pressure distribution and average pressure solution, normal deformation and average film thickness solution and computing leakage rate respectively. The results showed that seal operation depends not only on seal design but also on the history of the seal.

Thatte and Salant [14] presented a study on transient elastohydrodynamic lubrication analysis of an elastomeric hydraulic seal. Since reciprocating hydraulic rod seals generally operate with mixed lubrication in contact area, this type of seals has varying parameters to analyze. In this study, the effect of varying rod speed on seal is analyzed by developing a transient numerical model. A finite volume solution of the Reynolds equation using a mass-conserving algorithm is given for the analysis of the lubricating

film of hydraulic fluid. A contact mechanics analysis of the contacting asperities on the seal lip and a structural analysis of the seal deformations are performed. The lubricating film thickness, contact pressure and fluid pressure distributions, the friction force on the rod and the instantaneous flow rate are presented due to the cyclic histories. Computational procedure is given also. The results showed that a transient elastohydrodynamic lubrication analysis can reveal the history of a reciprocating seal's behavior over a cycle.

Kasem [15] presented a numerical analysis of leakage rate for the selection of elastomeric sealing materials. The leakage depends on many factors, such as the seal material, temperature, driving pressure, seal compression and seal geometry. Leakage rate of seals are investigated for six different elastomeric materials by using the viscoelastic properties of the materials.

In another study, Salant and Flaherty [16] presented an analysis of reverse pumping in rotary lip seals by taking into account microundulations on the seal surface. The elastic behavior of the lip and the fluid mechanics of the lubricating film are studied numerically. The pressure and shear stress distributions of the lubricating film and leakage flow are determined by the fluid mechanics of the film which is governed by the Reynolds equation. The elastic deformation occurs on the lip due to the film thickness distribution. The analysis shows that, under dynamic conditions, the undulation pattern deforms such that it produces reverse pumping.

Yang, YungWen, ShiangTseng [17] studied on a direct numerical simulation model to analyze the pumping mechanism of a radial lip seal with helical ribs. Ribbed seals are new types of rotary lip seals which obtain a better sealing performance. The flow field around the contact region between the seal lip and the shaft surface in the environment of a pumping rate test rig, where both air and oil sides are filled with oil initially, was

simulated. A three-dimensional finite element structure analysis of a ribbed helix seal is developed. The current results demonstrate that it is possible to achieve a substantial reduction in development and testing time with the promising application of CFD in the design of ribbed helix lip seals.

A complete mixed lubrication model for mechanical face seals with plain faces is presented by Lebeck [18]. This model is necessary to predict the seal leakage and the friction power as functions of the face profile and the operating conditions. for the purposes of design and analysis of plain-face contacting mechanical face seals.

Load support is based on the sum of hydrostatic, hydrodynamic and contact pressure. Prediction of the hydrostatic pressure is straightforward. Empirical data are developed for the prediction of hydrodynamic load support. Both a plastic and an elastic model for contact pressure are presented. Load support, load support equilibrium and friction equations are presented. It is shown that the model is used to predict the film thickness and leakage for any combination of fluids and operating conditions.

2.3 Scope of the Thesis

In recent years interest, leakage problem in seals and the overall performance and efficiency of seals has placed more attention on elastohydrodynamic behaviors of seals. Radial lip seals are mounted on shafts with an initial interference and during running the oil film thickness between the shaft and the seal lip is very small and usually in the order of the shaft surface roughness. Therefore, in this thesis study, the effects of shaft surface roughness parameters and the seal undulation geometry on the oil leakage will be focused.

With this study, seal lip deformation and the average Reynolds equations in the modeling process are to be taken into account for the hydrodynamic pressure.

A computer program is to be developed to solve the elastohydrodynamic problem on lip seals by considering the surface roughness and lip deformation effects on hydrodynamic pressure and side leakage.

A literature survey and recent studies on the effect of shaft roughness on oil leakage in radial lip seals and the method of analysis required to perform is provided above. In Chapter three, for the elastohydrodynamic analysis, the governing equations for hydrodynamic lubrication for rough surfaces and the elastic deflection are introduced. In Chapter four, the numerical solution of the governing equations is described and an iterative procedure is given for the simultaneous solution of the equations. The verification of the developed software is carried out by comparing with the available results in the literature.

In the final chapter, the results for different case studies are revealed and discussed as they apply to a rotary lip seal together with the suggested future works.

CHAPTER 3

MODELING OF OIL LEAKAGE IN RADIAL LIP SEALS

In radial lip seals, under static conditions there is an interference fit between the lip seal and the shaft, resulting in a contact pressure distribution on the lip surface. However, under dynamic conditions there exists a thin lubricating oil film between the rotating shaft and the lip surface. The pressure distribution developed in the lubricating film deforms the lip in the radial direction which causes oil leakage between the lip surface and the shaft surface. In this chapter, the modeling of hydrodynamic pressure generation and deformation of seal and oil leakage is presented.

3.1 Radial Lip Seals

Lip seals are used between rotating and non-rotating machine components to prevent leakage through the contact interface from the sealed side to the air side and to prevent dirt from penetrating into the sealed region. Lip seals have been widely used in various applications such as rolling element bearings, internal combustion engines, hydraulic pumps etc. to seal the fluid in the presence of a rotating shaft and a non-rotating and/or reciprocating shaft. This is because they are compact, easily installed. The seal construction consists of two main components as seen in Figure 3.1. One of them is cylindrical outer covering of sheet steel (shell) or elastomer which seals statically against the housing bore and enables the requisite interference fit of the seal in the housing bore to be obtained as well as facilitating proper installation.

The second component is the sealing lip of elastomer which provides dynamic and static sealing against the shaft. The lip has a sealing edge which is formed by pressing, cutting or grinding and is normally pressed against the counterface on the shaft with a defined radial force by a garter spring. The edge of the sealing lip and the shaft counterface form the most important functional area of a radial shaft seal. The sealing effect of the lip can be enhanced by providing the contact area of the lip with hydrodynamic aids which may be designed for single direction operation, or for alternating directions of shaft rotation.

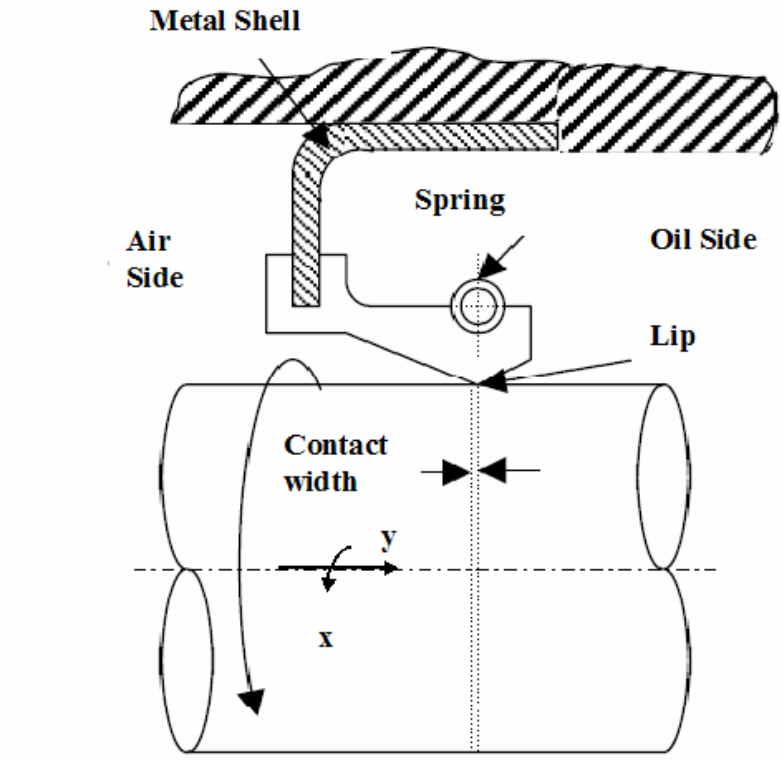

Figure 3.1 Rotary Lip Seal mounted on a shaft

3.2 Hydrodynamic Lubrication

Hydrodynamic lubrication is modeled by Reynolds equation for smooth surfaces. Rough surface effects on Reynolds equation are investigated by using flow factors for Gaussian surfaces and non-Gaussian surfaces separately.

3.2.1 Reynolds Equation for Smooth Surfaces

The differential equation governing pressure distribution in a lubricant film was obtained by Reynolds in 1886. The Reynolds' equation can be derived with the following assumptions;

1. The lubricant film thickness is much smaller than the nominal dimensions of the surfaces and the boundary surfaces are at a small angle with respect to each other and therefore pressure is constant across the lubricant film thickness.
2. Shear stress and velocity gradients are only significant across the lubricant film
3. The lubricant is incompressible and Newtonian.
4. The lubricant flow is laminar.
5. The bounding surfaces are considered to be isothermal, so that there is no temperature rise caused by conductive heat transfer to them. Also, the oil film is considered to be so thin that there is no convective heat transfer either.
6. The lubricant viscosity is constant in the film.
7. Inertia and surface tension forces are negligible compared with viscous forces.
8. The boundary surfaces are rigid and smooth with no surface micro-asperities.
9. No slip at the boundary surfaces.

Using the assumptions listed above and knowing that the film thickness is in the order of 10^{-3} of the surface dimensions, the fluid velocity normal to the surfaces would be

neglected. Then, the Reynolds Equation for smooth surfaces is derived by simplifying the Navier Stokes equations in association with continuity equation.

Figure 3.2 shows two surfaces separated by a fluid film. The coordinate system represented on the lower surface. Fluid film thickness is represented as h(x,y). The upper surface is stationery and lower surface is assumed as moving at a velocity of U in the x-direction.

Flow per unit length in x direction is given as

$$q_x = -\frac{h^3}{12\mu}\left(\frac{\partial p}{\partial x}+\frac{\partial p}{\partial y}\right)+\frac{Uh}{2}$$

Flow per unit length in y direction is given as

$$q_y = -\frac{h^3}{12\mu}\left(\frac{\partial p}{\partial x}+\frac{\partial p}{\partial y}\right)$$

The steady flow continuity equation is

$$\frac{\partial q_x}{\partial y}+\frac{\partial q_y}{\partial y}=0$$

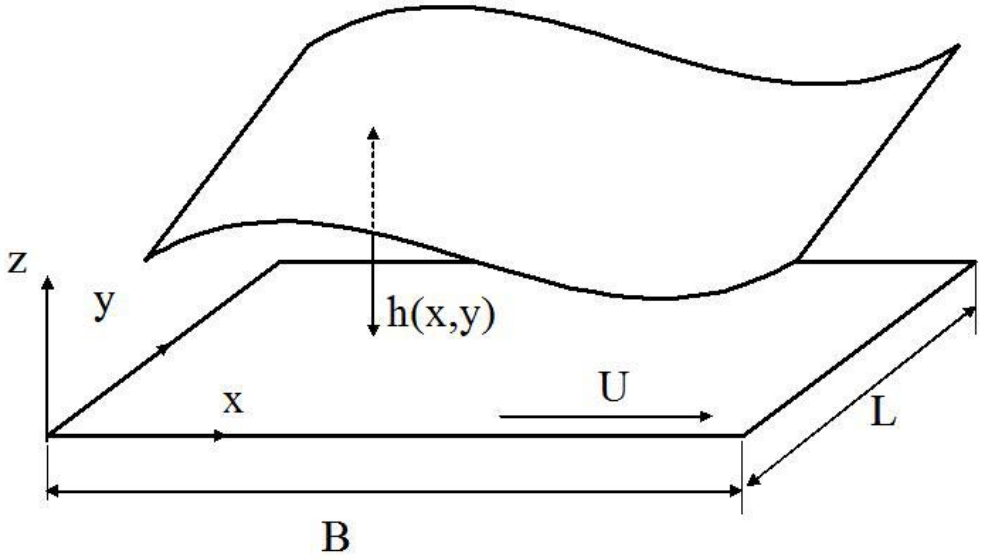

Figure 3.2 Coordinate system for Reynolds Equation

The general form of Reynolds' equation can be derived using steady flow continuity equation for the configuration shown in Figure 3.2:

$$\frac{\partial}{\partial x}\left(h^3\frac{\partial p}{\partial x}\right)+\frac{\partial}{\partial y}\left(h^3\frac{\partial p}{\partial y}\right)=6\mu U\frac{\partial h}{\partial x}+12\mu\frac{\partial h}{\partial t} \qquad (3.1)$$

where μ is the fluid viscosity. For steady state condition, the time derivative of film thickness on the right-hand side drops.

For the solution of the Reynolds equation boundary conditions are to be applied. The pressure values at the sides are equal to atmospheric pressure and taken as zero.

$$p(x,0)=0,\ p(x,L)=0,\ p(0,y)=0,\ p(B,y)=0$$

At the regions where there is diverging film in the direction of sliding, the oil film ruptures due to pressure drop and forms the cavitation region. In the cavitation zone where pressure drops below the atmospheric pressure, it is taken as the atmospheric pressure and the Reynolds boundary conditions are considered. That is p=0, dp/dx=dp/dy=0.

3.2.2 Average Reynolds Equation for Rough Surfaces

Engineering surfaces have asperities resulting from different manufacturing processes or because of running-in. As the mean oil film thickness between the surfaces approaches the height of asperities, like in radial lip seals, the oil flow through the channels between asperities becomes important. Therefore, a straight forward application of the Reynolds equation for smooth surfaces requires a detailed description of surface asperities.

When partial lubrication is present the texture of the asperity contacts affect the oil flow through the clearance of lubricated surfaces. An average Reynolds equation for rough surface is defined to analyze roughness effects on the flow. The average flow equation is derived through flow simulation which is based on numerically solving the Reynolds equation on a model bearing with a randomly generated surface roughness and then deriving the average Reynolds equation from the mean flow quantities.

Patir and Cheng [3] considered the effect of an assumed undistorted surface roughness layer on the elastohydrodynamic lubrication of the system by using the average Reynolds equation with flow factors. The average Reynolds equation is

$$\frac{\partial}{\partial x}\left(\phi_x \frac{h^3}{12\mu}\frac{\partial p}{\partial x}\right)+\frac{\partial}{\partial y}\left(\phi_y \frac{h^3}{12\mu}\frac{\partial p}{\partial y}\right)=\frac{U}{2}\frac{\partial h}{\partial x}+\frac{U\sigma}{2}\frac{\partial \phi_s}{\partial x} \qquad (3.2)$$

where h is the nominal film thickness, ϕ_x and ϕ_y are the pressure flow factors which modify the flow along the x and y directions due to the roughness and ϕ_s is the shear flow factor. Equation (3.2) can be non-dimensionalized using the following parameters.

$$X = \frac{x}{B}, \qquad Y = \frac{y}{L}, \qquad H = \frac{h}{\sigma}, \qquad P = \frac{p}{6\mu UB/\sigma^2}$$

B : width of slider bearing along the sliding direction

L : length of slider bearing in the transverse direction

σ : roughness

U : velocity of slider ($U=U_1$)

μ : absolute viscosity

The Reynolds equation with non-dimensional parameters for rough surfaces using the flow factors is given as

$$\frac{\partial}{\partial X}\left(\phi_x H^3 \frac{\partial P}{\partial X}\right) + \left(\frac{B}{L}\right)^2 \frac{\partial}{\partial Y}\left(\phi_y H^3 \frac{\partial P}{\partial Y}\right) = \frac{\partial H}{\partial X} + \frac{\partial \phi_s}{\partial X} \tag{3.3}$$

The Reynolds equation being a second order two-dimensional elliptic type differential equation can be solved for a given film thickness and L/B ratio.

3.2.3 Flow Factors for Gaussian Surfaces

The pressure flow factors were obtained through 1-D numerical flow simulation across small randomly generated Gaussian roughness which can simulate different types of asperity geometry. For a given surface roughness characteristics, the flow coefficients

are calculated statistically by Patir and Cheng [3] for the model shown in Figure 3.3 under a pressure drop.

In this model, it is assumed that the bearing is approximated by a number of small rectangular bearings of area δA_i as seen in Figure 3.4 and the film thickness between the surfaces is assumed as constant h.

The boundary conditions are as follows.

1. $p = p_A$ at x=0
2. $p = p_B$ at x=Lx
3. $\frac{\partial p}{\partial y} = 0$ at y=0, y=Ly
4. No flow at contact points

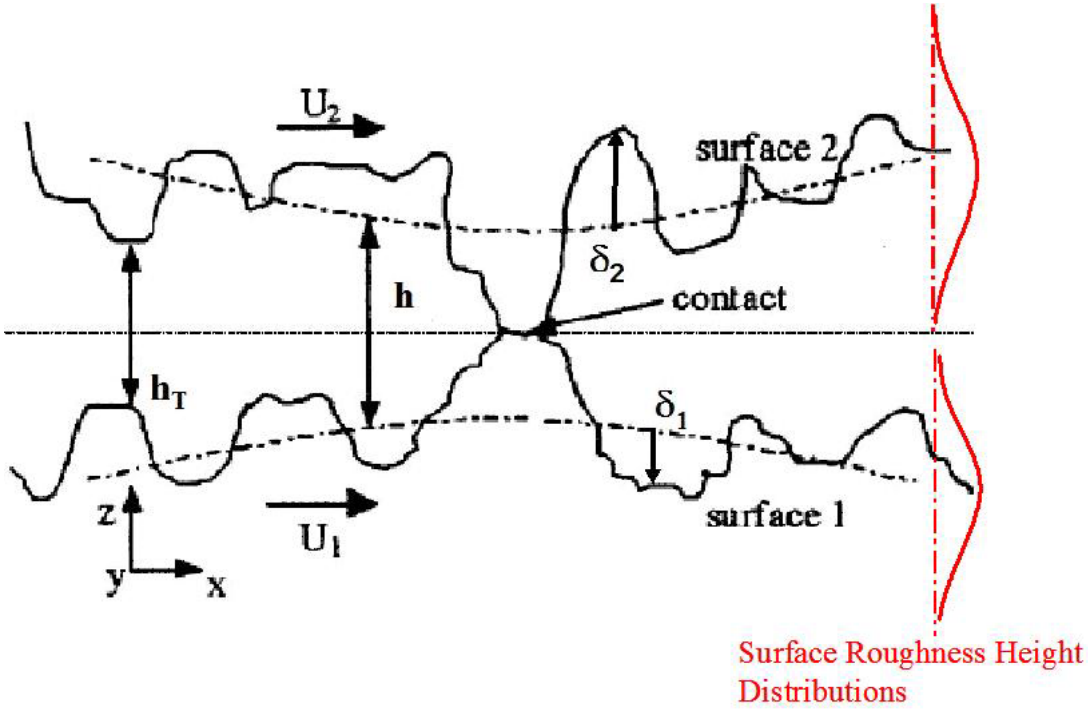

Figure 3.3 Rough surfaces in sliding and film thickness variation

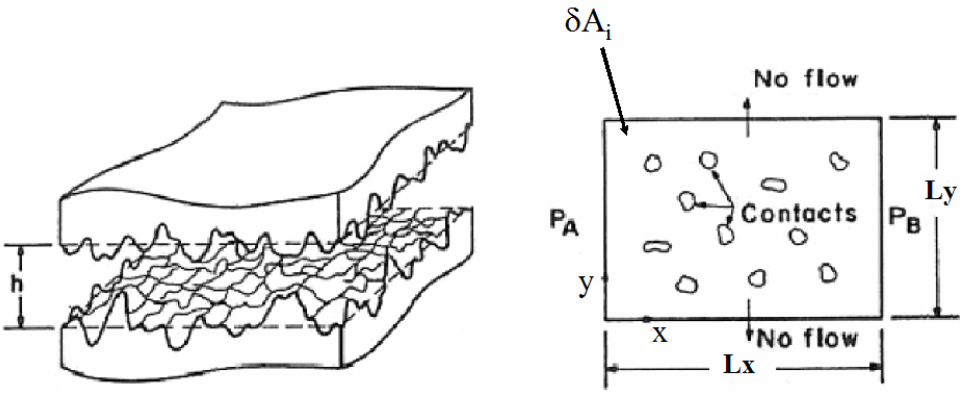

Figure 3.4 Rough Surface Model for simulation of ϕ_x and ϕ_y (Patir and Cheng [3])

The contacts of a general three dimensional surface that is partially lubricated can be modeled as ellipses with the mean ellipticity ratio γ which is also known as Peklenik number. Flow factors are dependent on ellipticity ratio and nominal film thickness. The asperity shapes are mostly in the longitudinal or transverse directions as shown in Figure 3.5. Longitudinally oriented contact areas ($\gamma > 1$), offer little resistance to the pressure flow, permitting only a small side flow. Patterns which are purely transverse, isotropic or longitudinal to the entrainment flow correspond to $\gamma = 0$, 1 or infinity, respectively.

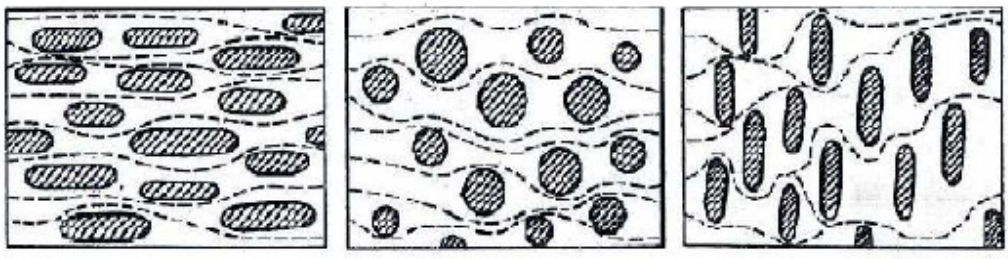

$\gamma > 1$ $\gamma = 1$ $\gamma < 1$

Figure 3.5 Typical contact areas for longitudinally oriented ($\gamma > 1$), isotropic ($\gamma = 1$) and transversely oriented ($\gamma < 1$) surfaces (Patir and Cheng [3])

Flow factors are function of the parameter h/σ in Patir and Cheng [3]. The pressure flow factors are calculated and expressed by the equations given below.

$$\phi_x = 1 - Ce^{-rH} \quad \text{for } \gamma \le 1$$

$$\phi_x = 1 + CH^{-r} \quad \text{for } \gamma > 1$$

where

$$H = \frac{h}{\sigma}$$

The constants C and r are given as functions of γ in Table 3.1.

The flow factor in y-direction, ϕ_y, is expressed as $\phi_y(H,\gamma) = \phi_x\left(H,1/\gamma\right)$

Table 3.1 Coefficients of equations for ϕ_x (Patir and Cheng [3])

γ	C	r	Range
1/9	1.48	0.42	H > 1
1/6	1.38	0.42	H > 1
1/3	1.18	0.42	H >0 .75
1	0.90	0.56	H > 0.5
3	0.225	1.5	H >0 .5
6	0.520	1.5	H > 0.5
9	0.870	1.5	H >0 .5

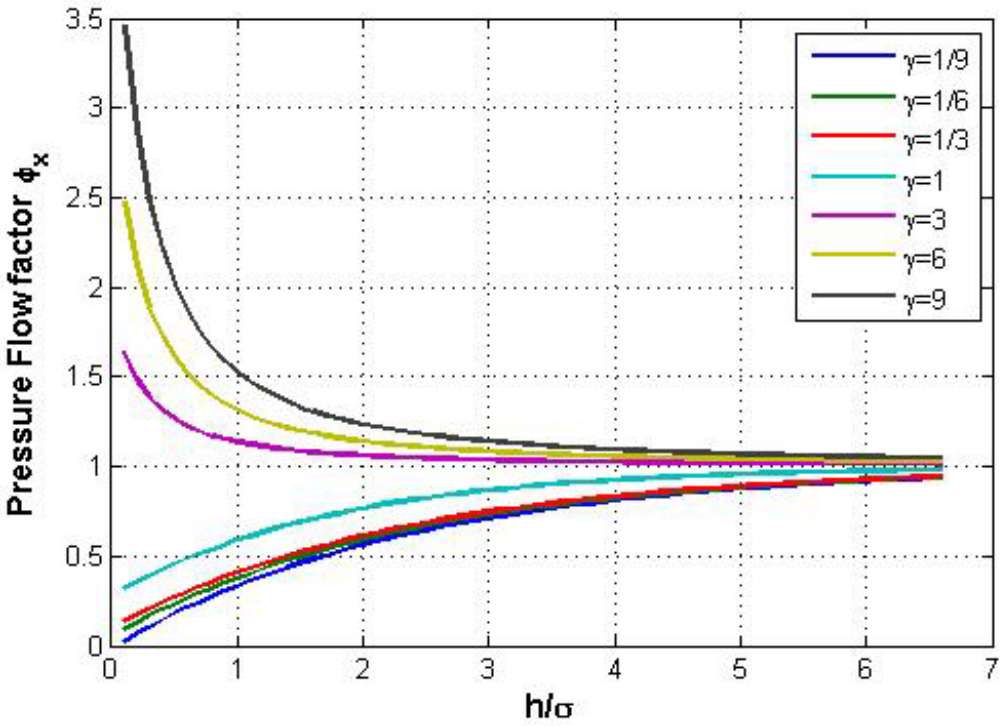

Figure 3.6 Pressure Flow Factors given by Patir and Cheng [3]

The shear flow factor $\Phi_{s,}$ is a function of the film thickness, the standard deviations and the surface pattern parameters of the two opposing surfaces.

$$\phi_s = V_{r1}\Phi_s\left(\frac{h}{\sigma},\gamma_1\right) - V_{r2}\Phi_s\left(\frac{h}{\sigma},\gamma_2\right)$$

And V_{r1} and V_{r2} are the variance ratios given as

$$V_{r1} = \left(\frac{\sigma_1}{\sigma}\right)^2, \quad V_{r2} = \left(\frac{\sigma_2}{\sigma}\right)^2 = 1 - V_{r1}$$

The Φ_s values are expressed by the equations given below (Patir and Cheng [3]).

$$\Phi_s = A_1 H^{\alpha_1} e^{-\alpha_2 H + \alpha_3 H^2} \qquad \text{for} \quad H \le 5$$

$$\Phi_s = A_2 e^{-0.25H} \qquad \text{for} \quad H > 5$$

The constants A_1, A_2, α_1, α_2, α_3 given as functions of γ in Table 3.2.

Table 3.2 Coefficients of equations for Φ_s (Patir and Cheng [3])

γ	A_1	α_1	α_2	α_3	A_2
1/9	2.046	1.12	0.78	0.03	1.856
1/6	1.962	1.08	0.77	0.03	1.754
1/3	1.858	1.01	0.76	0.03	1.561
1	1.899	0.98	0.92	0.05	1.126
3	1.560	0.85	1.13	0.08	0.556
6	1.290	0.62	1.09	0.08	0.388
9	1.011	0.54	1.07	0.08	0.295

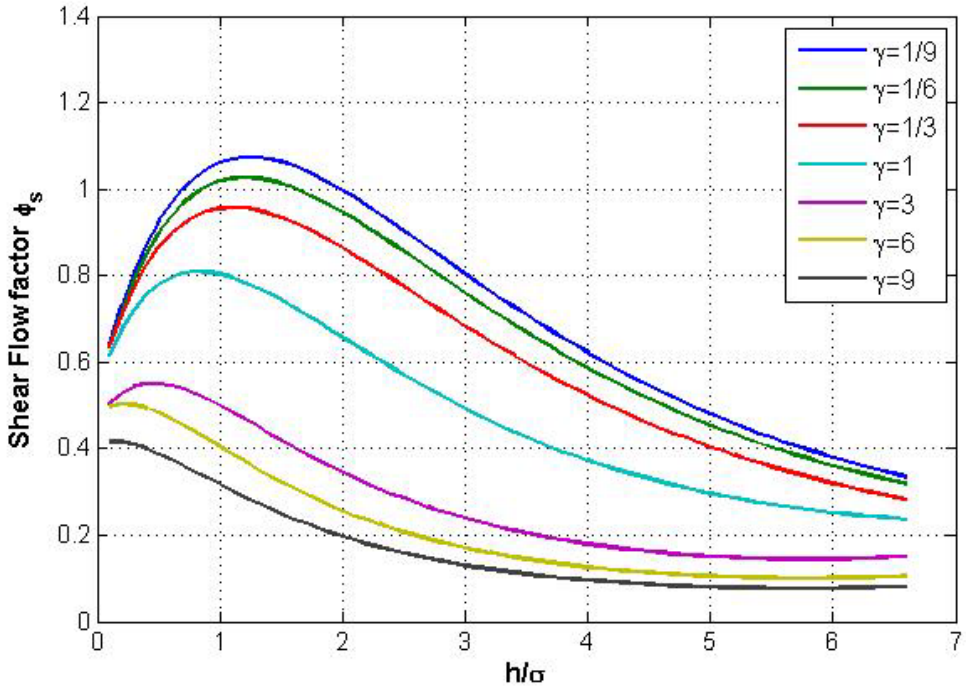

Figure 3.7 Shear Flow Factors given by Patir and Cheng [3]

3.2.4 Flow Factors for Non-Gaussian Surfaces

Patir and Cheng [3] derived pressure and shear flow factors for a rough surface with Gaussian height distribution. Their idea is improved and modified by Morales and Espejel [10] to derive pressure and shear flow factors for non-Gaussian surfaces. Morales-Espejel [10] presented a simple analytical approximation to derive pressure and shear flow factors for non-Gaussian surfaces in terms of Gaussian flow factors.

In this study, $\hat{\phi}$ is defined as the pressure flow factor for non-Gaussian roughness and ϕ' as the pressure flow factor for a Gaussian roughness.

$$\hat{\phi} = \phi' + \left(\frac{\sigma}{h}\right)^3 S_k \qquad \gamma \geq 1 \qquad (3.4)$$

$$\hat{\phi} = \frac{1}{\frac{1}{\phi'} + (1-\gamma)^n N_g} \qquad \gamma < 1 \tag{3.5}$$

$$N_g = -10\left(\frac{\sigma}{h}\right)^3 S_k + 15\left(\frac{\sigma}{h}\right)^4 (K-3)$$

where

σ : Standard deviation of the roughness heights

h : Film thickness

S_k : Normalized skewness of the heights

γ : Peklenik number

K : Kurtosis

n is a constant which makes N_g disappear when $\gamma \rightarrow 1$ for $n \neq 0$. For non-Gaussian rough surfaces, the variation of pressure flow factors as modified with the application of Equations (3.4) and (3.5) are shown in Figures 3.8a and 3.8b, respectively. Note that both Equations (3.4) and (3.5) reduces to Gaussian flow factors for Sk=0 and K=3.

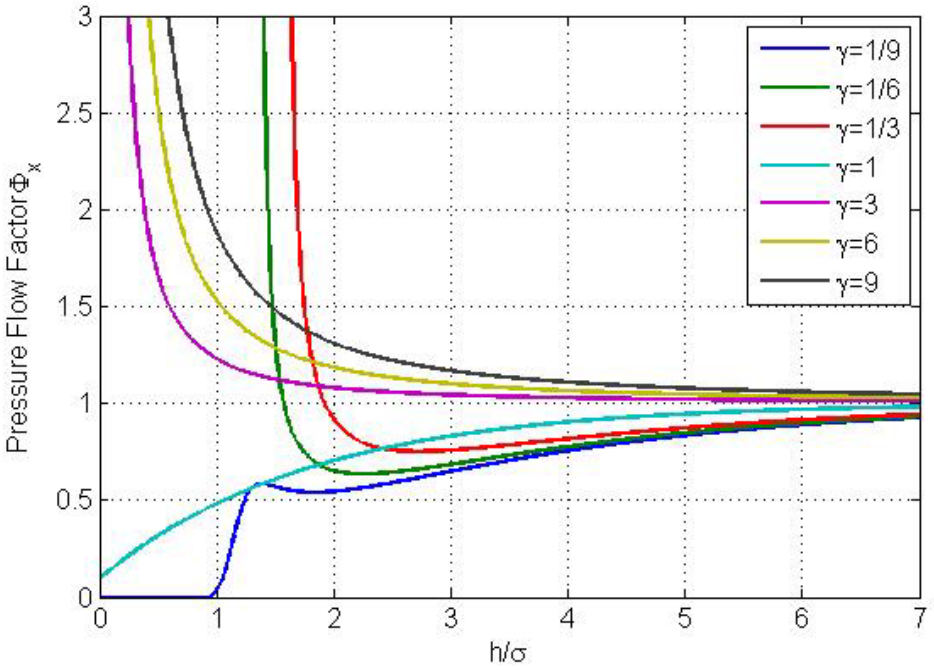

a) for Sk = 0, K = 2

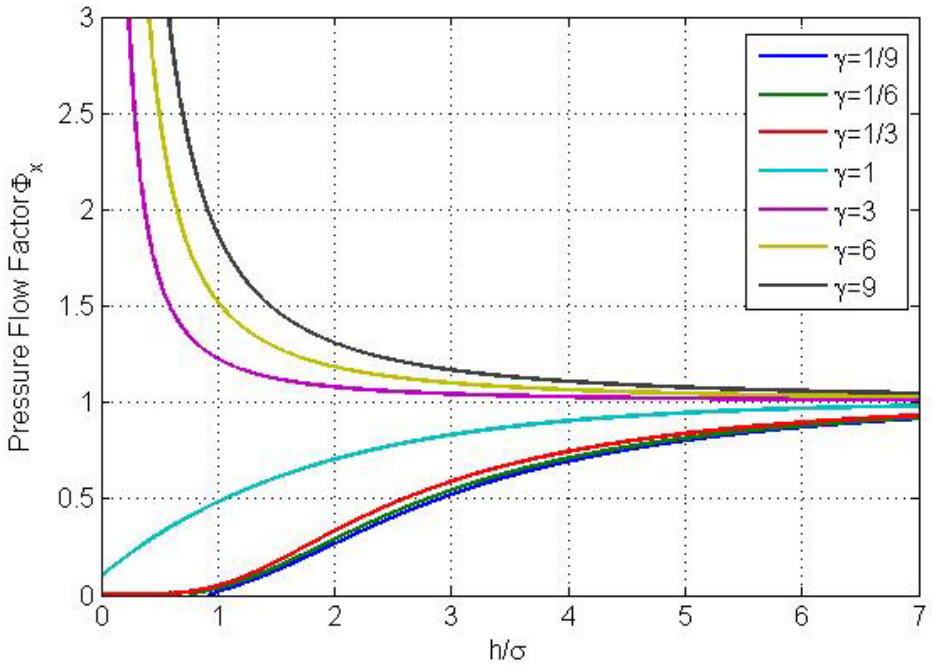

b) for Sk = 0, K = 4

Figure 3.8 Variation of pressure flow factors for non-Gaussian surfaces for n = 0

The shear flow factors are modified by Equation 3.6 for Patir Cheng [3] results for isotropic surfaces (γ =1). For non-Gausssian surfaces the following approximation is suggested by Morales-Espejel [10]

$$\hat{\phi}_s = \phi'_s \left(\frac{1 + N_{g1}/g_1}{1 + N_{g2}/g_2} \right) \tag{3.6}$$

where

$$N_{g1} = 6\left(\frac{\sigma}{h}\right)^2 S_k - 10\left(\frac{\sigma}{h}\right)^3 (K-3)$$

$$N_{g2} = -10\left(\frac{\sigma}{h}\right)^3 S_k + 150(\gamma)\left(\frac{\sigma}{h}\right)^4 (K-3)$$

$$g_1 = -3\left(\frac{\sigma}{h}\right) - 30\left(\frac{\sigma}{h}\right)^3$$

$$g_2 = 1 + 6\left(\frac{\sigma}{h}\right)^2 + 450(\gamma)\left(\frac{\sigma}{h}\right)^4$$

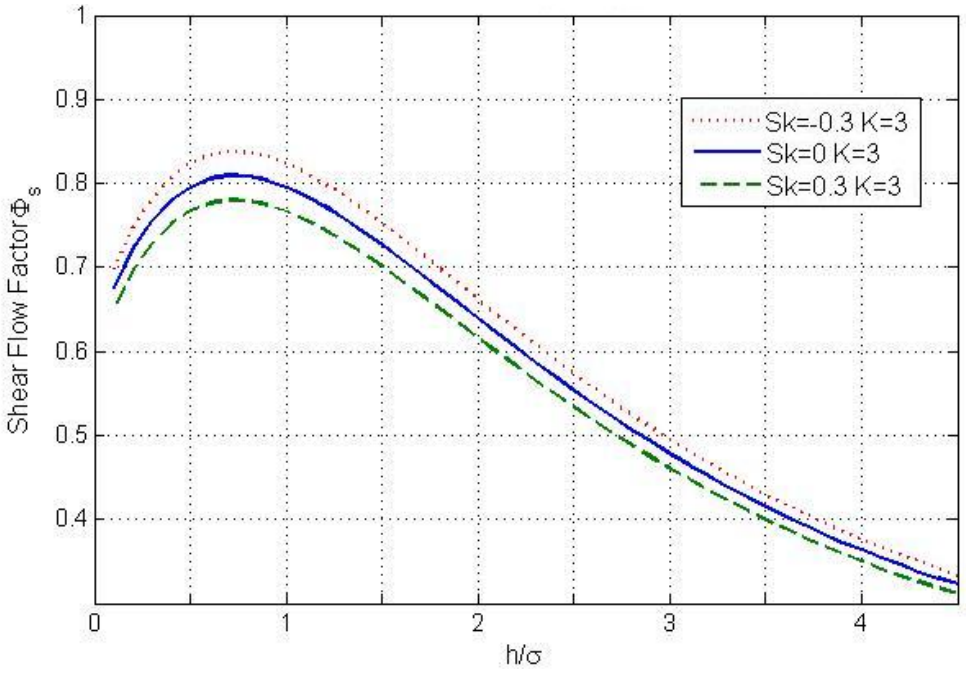

a) For K=3

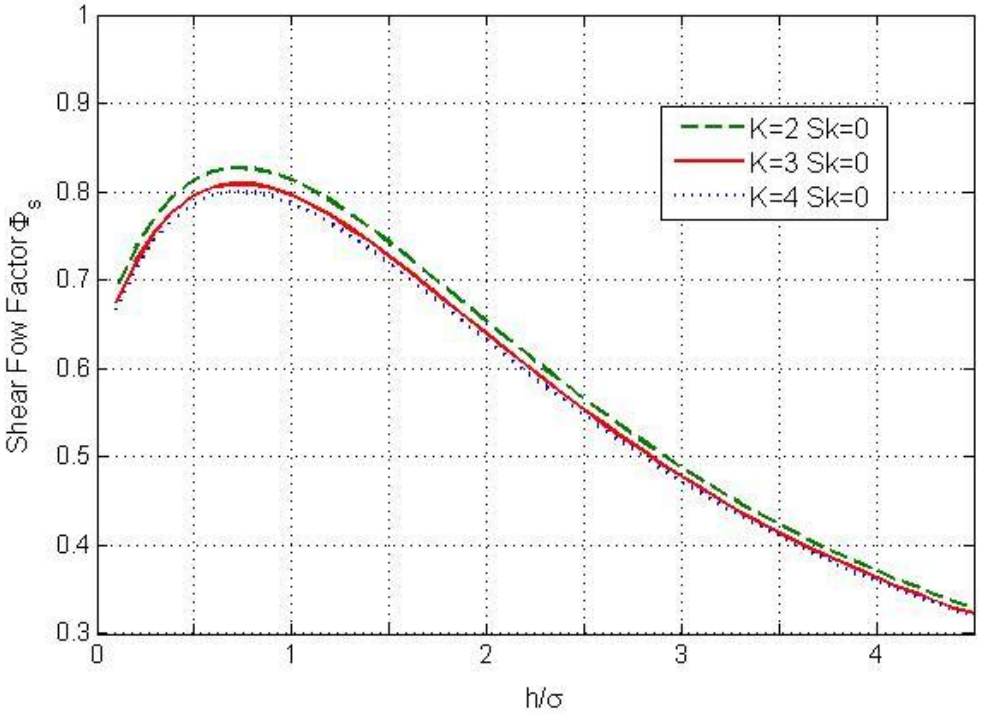

b) For S_k=0

Figure 3.9 Variation of shear flow factor for non-Gaussian surfaces for γ=1

3.3 Elastic Deformation Analysis

For two contiguous elastic bodies loaded against each other or separated by a thin elastohydrodynamic film where the pressure distribution is known, if the surfaces are assumed to be smooth, that is, their roughness values are so small compared to elastic deformation of surfaces, the total deflection is given as (Gohar [19])

$$\delta(x,y) = \frac{1}{E_r}\iint_A \frac{p(x_1,y_1)dx_1dy_1}{\sqrt{(x-x_1)^2+(y-y_1)^2}} \tag{3.7}$$

Referring to Figure 3.10, p is the lubricant pressure at (x_1, y_1) and acts over an elementary area dx_1dy_1 of each body surface, δ is the sum of the two individual deflections at (x,y) due to the distribution of p(x_1, y_1) over footprint area A of the surfaces, and E_r is the reduced Young's modulus, which can be obtained from the expression:

$$\frac{1}{E_r} = \frac{1}{\pi}\left\{\frac{1-v_1^{\,2}}{E_1} + \frac{1-v_2^{\,2}}{E_2}\right\} \tag{3.8}$$

where E_1 and E_2 are the Young's modules, v_1 and v_2 are the poisons ratios of the surface materials.

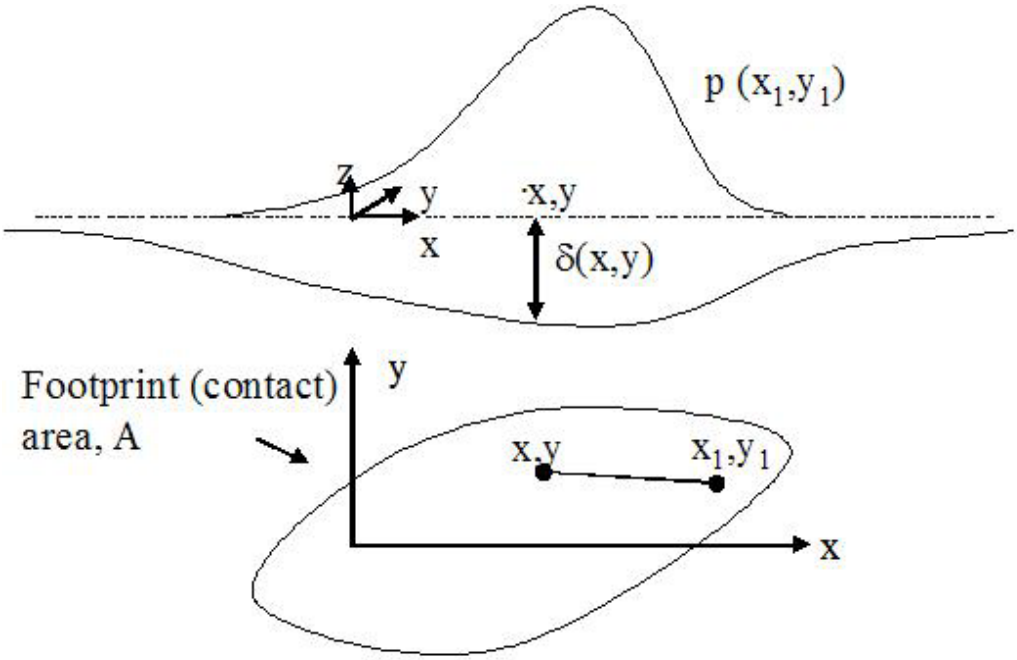

Figure 3.10 Elastic Deformation Sketch

3.4 Analysis of Oil Leakage

Due to the hydrodynamic pressure distribution across the contact width of the lip in Figure 3.1, oil leakage occurs at the lip edge through the air side in the axial direction. For the film thickness at the lip edge h between the shaft and the lip, the side flow per unit width in the y-direction is given as

$$q_y = -\left|\frac{h^3}{12\mu}\frac{\partial p}{\partial y}\right|_{y=L} \tag{3.9}$$

where L is the contact width, h is the film thickness at the lip edge and p is the pressure distribution.

For an infinitesimal element which has a thickness of dx at the lip edge, the side flow is

$$dq = q_y dx = -\left|\frac{h^3}{12\mu}\frac{\partial p}{\partial y}\right|_{y=L} dx$$

Integration of both sides of the equation gives the total side flow as

$$q = \int_0^B q_y dx = -\frac{1}{12\mu}\int_0^B \left|h^3 \frac{\partial p}{\partial y}\right|_{y=L} dx \qquad (3.10)$$

Using the non-dimensional parameters as

$$H = \frac{h}{\sigma}, \quad X = \frac{x}{B}, \quad Y = \frac{y}{L}, \quad P = \frac{p}{6\mu UB/\sigma^2},$$

$$LD = \frac{L}{B}, \quad Q = \frac{q}{\sigma BU/2}$$

Then, the non-dimensional flow equation becomes

$$Q = -\frac{1}{LD}\int_0^1 \left|H^3 \frac{\partial P}{\partial Y}\right|_{Y=1} dX \qquad (3.11)$$

CHAPTER 4

SIMULATION OF OIL LEAKAGE IN RADIAL LIP SEALS

In this chapter, the methods of numerical solution of the mathematical equations given in Chapter 3 and the computational procedure are presented. The computer program developed involves three basic steps; numerical solutions of Reynolds equation for rough surfaces, radial lip seal deformation due to hydrodynamic pressure developed and the oil flow leakage on the edge of the lip. The computational algorithm and the computer program developed is given for the simultaneous solution of the hydrodynamic flow and the elastic deformation of the lip.

4.1 Finite Difference Solution of Reynolds Equation for Rough Surfaces

The non-dimensional Reynolds equation for rough surfaces given in Equation 3.3 is arranged in terms of the first and second derivatives of unknown pressure

$$\phi_X\left(H^3\frac{\partial^2 P}{\partial X^2}+3H^2\frac{\partial H}{\partial X}\frac{\partial P}{\partial X}\right)+\left(\frac{B}{L}\right)^2\phi_Y\left(H^3\frac{\partial^2 P}{\partial Y^2}+3H^2\frac{\partial H}{\partial Y}\frac{\partial P}{\partial Y}\right)$$
$$+H^3\frac{\partial P}{\partial X}\frac{\partial \phi_X}{\partial H}\frac{\partial H}{\partial X}+\left(\frac{B}{L}\right)^2 H^3\frac{\partial P}{\partial Y}\frac{\partial \phi_Y}{\partial H}\frac{\partial H}{\partial Y}=\frac{\partial H}{\partial X}+\frac{\partial \phi_s}{\partial X}$$

By dividing the both sides of the equation by H^3 gives

$$\phi_X\left(\frac{\partial^2 P}{\partial X^2}+\frac{3}{H}\frac{\partial H}{\partial X}\frac{\partial P}{\partial X}\right)+\left(\frac{B}{L}\right)^2\phi_Y\left(\frac{\partial^2 P}{\partial Y^2}+\frac{3}{H}\frac{\partial H}{\partial Y}\frac{\partial P}{\partial Y}\right)$$
$$+\frac{\partial P}{\partial X}\frac{\partial \phi_X}{\partial H}\frac{\partial H}{\partial X}+\left(\frac{B}{L}\right)^2\frac{\partial P}{\partial Y}\frac{\partial \phi_Y}{\partial H}\frac{\partial H}{\partial Y}=\frac{1}{H^3}\left(1+\frac{\partial \phi_s}{\partial H}\right)\frac{\partial H}{\partial X}$$

and rearranging the terms gives the coefficients of the derivatives of pressure as

$$\left(\phi_X\frac{\partial^2 P}{\partial X^2}+\left(\frac{B}{L}\right)^2\phi_Y\frac{\partial^2 P}{\partial Y^2}\right)+\left(\frac{3\phi_X}{H}\frac{\partial H}{\partial X}+\frac{\partial \phi_X}{\partial H}\frac{\partial H}{\partial X}\right)\frac{\partial P}{\partial X}$$
$$+\left(\frac{B}{L}\right)^2\left(\frac{3\phi_Y}{H}\frac{\partial H}{\partial Y}+\frac{\partial \phi_Y}{\partial H}\frac{\partial H}{\partial Y}\right)\frac{\partial P}{\partial Y}=\frac{1}{H^3}\left(1+\frac{\partial \phi_s}{\partial H}\right)\frac{\partial H}{\partial X}$$

For numerical solution of the Reynolds equation, the finite difference form of the equation is required.

Using standard central finite difference approximations, the first and second derivatives of the pressure can be expressed as

$$\frac{\partial P}{\partial X}=\frac{P_{i+1,j}+P_{i-1,j}}{2\Delta X}$$
$$\frac{\partial^2 P}{\partial X^2}=\frac{P_{i+1,j}-2P_{i,j}+P_{i-1,j}}{\Delta X^2}$$
$$\frac{\partial P}{\partial Y}=\frac{P_{i+1,j}+P_{i-1,j}}{2\Delta Y}$$
$$\frac{\partial^2 P}{\partial Y^2}=\frac{P_{i+1,j}-2P_{i,j}+P_{i-1,j}}{\Delta Y^2}$$

Using the finite difference approximations for the derivatives, the Reynolds equation takes the following form.

$$\left(\phi_X \frac{P_{i+1,j} - 2P_{i,j} + P_{i-1,j}}{\Delta X^2} + \left(\frac{B}{L}\right)^2 \phi_Y \frac{P_{i+1,j} - 2P_{i,j} + P_{i-1,j}}{\Delta Y^2}\right)$$
$$+\left(\frac{\partial \phi_X}{\partial H} + \frac{3\phi_X}{H}\right)\frac{\partial H}{\partial X}\left(\frac{P_{i+1,j} + P_{i-1,j}}{2\Delta X}\right)$$
$$+\left(\frac{B}{L}\right)^2\left(\frac{\partial \phi_Y}{\partial H} + \frac{3\phi_Y}{H}\right)\frac{\partial H}{\partial Y}\left(\frac{P_{i+1,j} + P_{i-1,j}}{2\Delta Y}\right)$$
$$= \frac{1}{H^3}\left(1 + \frac{\partial \phi_S}{\partial H}\right)\frac{\partial H}{\partial X}$$

Rearrange the difference equation to solve for unknown $P_{i,j}$ in terms of the surrounding node values gives

$$2\left(\frac{\phi_X}{\Delta X^2} + \left(\frac{B}{L}\right)^2 \frac{\phi_Y}{\Delta Y^2}\right)P_{i,j} = \left(\phi_X \frac{P_{i+1,j} + P_{i-1,j}}{\Delta X^2} + \left(\frac{B}{L}\right)^2 \phi_Y \frac{P_{i,j+1} + P_{i,j-1}}{\Delta Y^2}\right)$$
$$+\left(\frac{\partial \phi_X}{\partial H} + \frac{3\phi_X}{H}\right)\frac{\partial H}{\partial X}\left(\frac{P_{i+1,j} + P_{i-1,j}}{2\Delta X}\right)$$
$$+\left(\frac{B}{L}\right)^2\left(\frac{\partial \phi_Y}{\partial H} + \frac{3\phi_Y}{H}\right)\frac{\partial H}{\partial Y}\left(\frac{P_{i,j+1} + P_{i,j-1}}{2\Delta Y}\right)$$
$$-\frac{1}{H^3}\left(1 + \frac{\partial \phi_S}{\partial H}\right)\frac{\partial H}{\partial X}$$

which can also be rearranged as

$$A_{i,j}P_{i,j} = \left(\phi_X \frac{P_{i+1,j} + P_{i-1,j}}{\Delta X^2}\right) + (ds)\frac{\partial H}{\partial X}$$
$$+\left(\left(\frac{B}{L}\right)^2 \phi_Y \frac{P_{i,j+1} + P_{i,j-1}}{\Delta Y^2} + \left(\frac{B}{L}\right)^2\left(\frac{\partial \phi_Y}{\partial H} + \frac{3\phi_Y}{H}\right)\left(\frac{P_{i,j+1} + P_{i,j-1}}{2\Delta Y}\right)\frac{\partial H}{\partial Y}\right)$$

where

$$A_{i,j} = 2\left(\frac{\phi_X}{\Delta X^2} + \left(\frac{B}{L}\right)^2 \frac{\phi_Y}{\Delta Y^2} \right)$$

$$ds = \left(\frac{\partial \phi_X}{\partial H} + \frac{3\phi_X}{H} \right)\left(\frac{P_{i+1,j} + P_{i-1,j}}{2\Delta X} \right) - \frac{1}{H^3}\left(1 + \frac{\partial \phi_S}{\partial H} \right)$$

Simply, the unknown pressure can be expressed as

$$A_{i,j} P_{i,j} = d + b \quad \text{or} \quad P_{i,j} = \frac{d+b}{A_{i,j}}$$

where

$$d = \left(\phi_X \frac{P_{i+1,j} + P_{i-1,j}}{\Delta X^2} \right) + (ds)\frac{\partial H}{\partial X}$$

$$b = \left(\left(\frac{B}{L}\right)^2 \phi_Y \frac{P_{i,j+1} + P_{i,j-1}}{\Delta Y^2} + \left(\frac{B}{L}\right)^2 \left(\frac{\partial \phi_Y}{\partial H} + \frac{3\phi_Y}{H} \right)\left(\frac{P_{i,j+1} + P_{i,j-1}}{2\Delta Y} \right)\frac{\partial H}{\partial Y} \right)$$

The pressure at any node i,j is evaluated by using the pressure values on the surrounding nodes. However, to accelerate the convergence, Successive Over Relaxation (SOR) method can be used with a Relaxation Factor (RF). After each iteration, calling the newly evaluated value for a node as

$$\left(P_{i,j}\right)_{new} = \frac{d+b}{A_{i,j}}$$

and the value on the previous iteration as

$$z = \left(P_{i,j}\right)_{old}$$

a better value for pressure $P_{i,j}$ can be assigned to accelerate the convergence using the following equation,

$$P_{i,j} = z + RF((P_{i,j})_{new} - z) = z + RF\left(\frac{d+b}{A_{i,j}} - z\right)$$

Where RF is the relaxation factor and determined by using numerical experimentation for the film geometry and L/B ratio. In this study it is taken as 1.7.

To check for convergence, in the computation domain the absolute weighted residual on pressure values is to be calculated for each iteration.

Summation of absolute residual $rs = \sum \left| |P_{j,i}| - z \right|$

Summation of absolute pressure in each $xs = \sum |P_{j,i}|$

Absolute weighted residual $ws = \frac{rs}{xs}$

The iterations continue until an acceptable value is reached on the absolute weighted residual. In this study, the absolute weighted residual is taken as 10^{-3}.

Boundary Conditions:

- The hydrodynamic pressures are along the seal edges are set to the ambient pressure.

- In the fluid film where the pressure may drop and the cavitation region may be formed, the size and the position are not known. Therefore, for the solution of the Reynolds equation with the Reynolds boundary condition, that is P=0, dP/dX=dP/dY=0 in the

cavitation region, are introduced into the numerical procedure by setting all sub-ambient pressures to zero during the iterative process. By that procedure the cavitation region satisfying the boundary conditions is determined.

4.2 Numerical Solution of Elastic Deflection Equation

If pressure is constant for a small rectangular element located on the origin of the coordinate system where c and d define the element boundaries from its centre as shown in Figure 4.1, Equation 3.7 is easily integrated to give deflection at any point (Gohar [19]).

The surfaces are assumed to be smooth, that is, their roughness values are so small compared to elastic deformation of surfaces as not to affect their elastic properties or the film hydrodynamics.

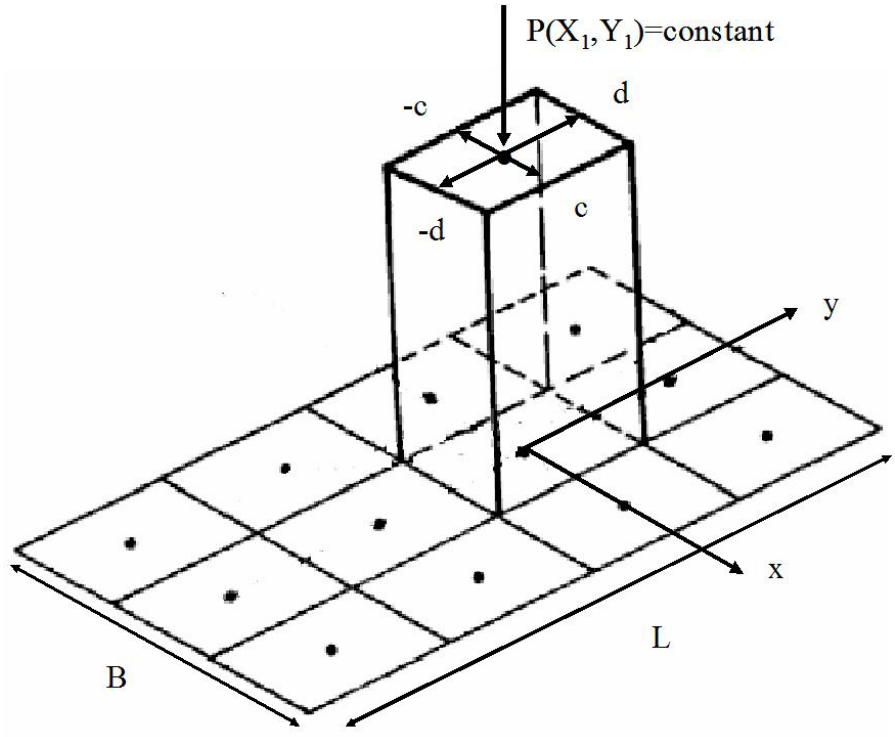

Figure 4.1 Flat-roofed element giving deflection at (x,y)

$$\delta(x,y)=\frac{p}{E_r}\left\{\begin{array}{l}(y-d)\ln\left[\dfrac{(x-c)+\sqrt{(y-d)^2+(x-c)^2}}{(x+c)+\sqrt{(y-d)^2+(x+c)^2}}\right]\\ +(y+d)\ln\left[\dfrac{(x+c)+\sqrt{(y+d)^2+(x+c)^2}}{(x-c)+\sqrt{(y+d)^2+(x-c)^2}}\right]\\ +(x+c)\ln\left[\dfrac{(y+d)+\sqrt{(y+d)^2+(x+c)^2}}{(y-d)+\sqrt{(y-d)^2+(x+c)^2}}\right]\\ +(x-c)\ln\left[\dfrac{(y-d)+\sqrt{(y-d)^2+(x-c)^2}}{(y+d)+\sqrt{(y+d)^2+(x-c)^2}}\right]\end{array}\right\} \tag{4.1}$$

Due to an arbitrary pressure distribution $p=p(x_k,y_l)$, for a small rectangular element located at (x_k,y_l), the deflection at any point (x,y) can be obtained by defining $x=x_i-x_k$ and $y=y_j-y_l$ in Equation 4.1. Then, due to the discrete elements, the total deflection at any point (x,y) can be expressed by the principle of elastic superposition

$$\delta_{ij}=\sum_{l=1}^{N}\sum_{k=1}^{M}I_{ij,kl}p_{kl} \tag{4.2}$$

where I is the influence coefficient matrix, M and N are the number of nodes in x and y directions, respectively. The subscripts k and l indicate the pressure value at x_k, y_l and i and j indicate any point in the region. Then, the influence coefficient becomes

$$I_{ij,kl} = \frac{1}{E_r}\left\{\begin{aligned}
&(y_j - y_l - d)\ln\left[\frac{(x_i - x_k - c) + \sqrt{(y_j - y_l - d)^2 + (x_i - x_k - c)^2}}{(x_i - x_k + c) + \sqrt{(y_j - y_l - d)^2 + (x_i - x_k + c)^2}}\right] \\
&+(y_j - y_l + d)\ln\left[\frac{(x_i - x_k + c) + \sqrt{(y_j - y_l + d)^2 + (x_i - x_k + c)^2}}{(x_i - x_k - c) + \sqrt{(y_j - y_l + d)^2 + (x_i - x_k - c)^2}}\right] \\
&+(x_i - x_k + c)\ln\left[\frac{(y_j - y_l + d) + \sqrt{(y_j - y_l + d)^2 + (x_i - x_k + c)^2}}{(y_j - y_l - d) + \sqrt{(y_j - y_l - d)^2 + (x_i - x_k + c)^2}}\right] \\
&+(x_i - x_k - c)\ln\left[\frac{(y_j - y_l - d) + \sqrt{(y_j - y_l - d)^2 + (x_i - x_k - c)^2}}{(y_j - y_l + d) + \sqrt{(y_j - y_l + d)^2 + (x_i - x_k - c)^2}}\right]
\end{aligned}\right\} \tag{4.3}$$

where $c = \frac{B}{2M}$, $d = \frac{L}{2N}$

In order to set up a numerical solution scheme, the governing equations should be non-dimensionalized. The choice of scaling factors will depend on the hydrodynamic problem being solved. Using the same non-dimensional parameters defined in Reynolds equation,

$$\bar{\delta} = \frac{\delta}{\sigma}, \quad P = \frac{p}{6\mu UB/\sigma^2}, \quad X = \frac{x}{B}, \quad Y = \frac{y}{L}, \quad \bar{c} = \frac{c}{B}, \quad \bar{d} = \frac{d}{L}, \quad \bar{I}_{ij,kl} = \frac{I_{ij,kl}}{B}$$

the non-dimensional influence coefficient matrix becomes

$$\bar{I}_{i,j,k,l} = \left\{ \begin{aligned} & \frac{L}{B}(Y_j - Y_l - \bar{d}) \ln \left[\frac{(X_i - X_k - \bar{c}) + \sqrt{\left(\frac{L}{B}\right)^2 (Y_j - Y_l - \bar{d})^2 + (X_i - X_k - \bar{c})^2}}{(X_i - X_k + \bar{c}) + \sqrt{\left(\frac{L}{B}\right)^2 (Y_j - Y_l - \bar{d})^2 + (X_i - X_k - \bar{c})^2}} \right] \\ & + \frac{L}{B}(Y_j - Y_l + \bar{d}) \ln \left[\frac{(X_i - X_k + \bar{c}) + \sqrt{\left(\frac{L}{B}\right)^2 (Y_j - Y_l + \bar{d})^2 + (X_i - X_k + \bar{c})^2}}{(X_i - X_k - \bar{c}) + \sqrt{\left(\frac{L}{B}\right)^2 (Y_j - Y_l + \bar{d})^2 + (X_i - X_k - \bar{c})^2}} \right] \\ & + (X_i - X_k + \bar{c}) \ln \left[\frac{\frac{L}{B}(Y_j - Y_l + \bar{d}) + \sqrt{\left(\frac{L}{B}\right)^2 (Y_j - Y_l + \bar{d})^2 + (X_i - X_k + \bar{c})^2}}{\frac{L}{B}(Y_j - Y_l - \bar{d}) + \sqrt{\left(\frac{L}{B}\right)^2 (Y_j - Y_l - \bar{d})^2 + (X_i - X_k + \bar{c})^2}} \right] \\ & + (X_i - X_k - \bar{c}) \ln \left[\frac{\frac{L}{B}(Y_j - Y_l - \bar{d}) + \sqrt{\left(\frac{L}{B}\right)^2 (Y_j - Y_l - \bar{d})^2 + (X_i - X_k - \bar{c})^2}}{\frac{L}{B}(Y_j - Y_l + \bar{d}) + \sqrt{\left(\frac{L}{B}\right)^2 (Y_j - Y_l + \bar{d})^2 + (X_i - X_k - \bar{c})^2}} \right] \end{aligned} \right\} \tag{4.4}$$

Then, the non-dimensionalized form of the elastic deflection equation becomes

$$\bar{\delta}_{ij,kl} = A \sum_{l=1}^{N} \sum_{k=1}^{M} \bar{I}_{ij,kl} P_{kl} \tag{4.5}$$

where the deformation parameter A is $A = \dfrac{6\mu U B^2}{E_r \sigma^3}$ (4.6)

4.3 Numerical Solution of Side Flow Equation

The numerical methods which are used for the solution of the flow equation (Eq. 3.11) are expressed below.

For the calculation of flow rate at oil side, backward difference method is used to evaluate the derivative term $\left.\frac{\partial P}{\partial Y}\right|_{Y=1}$, for the calculation of flow rate at air side forward difference is used to evaluate the derivative term $\left.\frac{\partial P}{\partial Y}\right|_{Y=0}$.

The 4th order backward difference expression for the first derivative of pressure:

$$\left.\frac{\partial P}{\partial Y}\right|_{Y=1} = \frac{-25P(i,M) + 48P(i,M-1) - 36P(i,M-2) + 16P(i,M-3) - 3P(i,M-4)}{12\Delta Y} \quad (4.7)$$

The 4th order forward difference expression for the first derivative of pressure:

$$\left.\frac{\partial P}{\partial Y}\right|_{Y=0} = \frac{-25P(i,0) + 48P(i,0+1) - 36P(i,0+2) + 16P(i,0+3) - 3P(i,0+4)}{12\Delta Y} \quad (4.8)$$

For the integration part of the flow equation (Equation 3.11), Simpson's rule is applied.

If multiplication of the pressure derivative at Y=0 for air side or Y=M for oil side and term of third order film thickness is called as function f:

$$f(i,M) = H(i,M)^3 \frac{-25P(i,M) + 48P(i,M-1) - 36P(i,M-2) + 16P(i,M-3) - 3P(i,M-4)}{12\Delta Y}$$

General form of the Simpson's rule is applied for side flow.

$$Q = -\frac{1}{LD}\int_0^1 \left| H^3 \frac{\partial P}{\partial Y}\right|_{Y=1} dX = -\frac{1}{LD}\frac{f(0,M) + \sum_{i+1}^{N-1}\{4f(i_{odd},M) + 2f(i_{even},M)\} + f(N,M)}{3\Delta X} \quad (4.9)$$

4.4 Computational Scheme for the Solution of Elastohydrodynamic Lubrication Equation

Since the hydrodynamics of the lubricating film and the structural mechanics are strongly coupled through the film thickness and the pressure developed, an iterative procedure is required to compute the performance of the seal. The computational procedure for the full elastohydrodynamic analysis is shown in Figure 4.2 and consists of two nested iteration loops. Solution of the pressure distribution in the lubricating film is obtained by using the initial guess for the film thickness, H, with convergence check. Once, the pressure distribution is converged, in the outer loop, the acquired pressure distribution is used to determine the seal lip deformation δ which is used to modify the oil film thickness, H, between the seal and the shaft surface. The pressure distribution in the lubricating film is recalculated in the inner loop with the new film thickness. The iterative process continues going back and forth between the inner and outer loops until the convergence criteria are satisfied for both the pressure distribution and the film thickness. Then, the simultaneous solution for the Reynolds equation and the deformation equations is reached and the oil leakage rate is calculated.

The program is developed using MATLAB and the listing of the program is given in Appendix A.

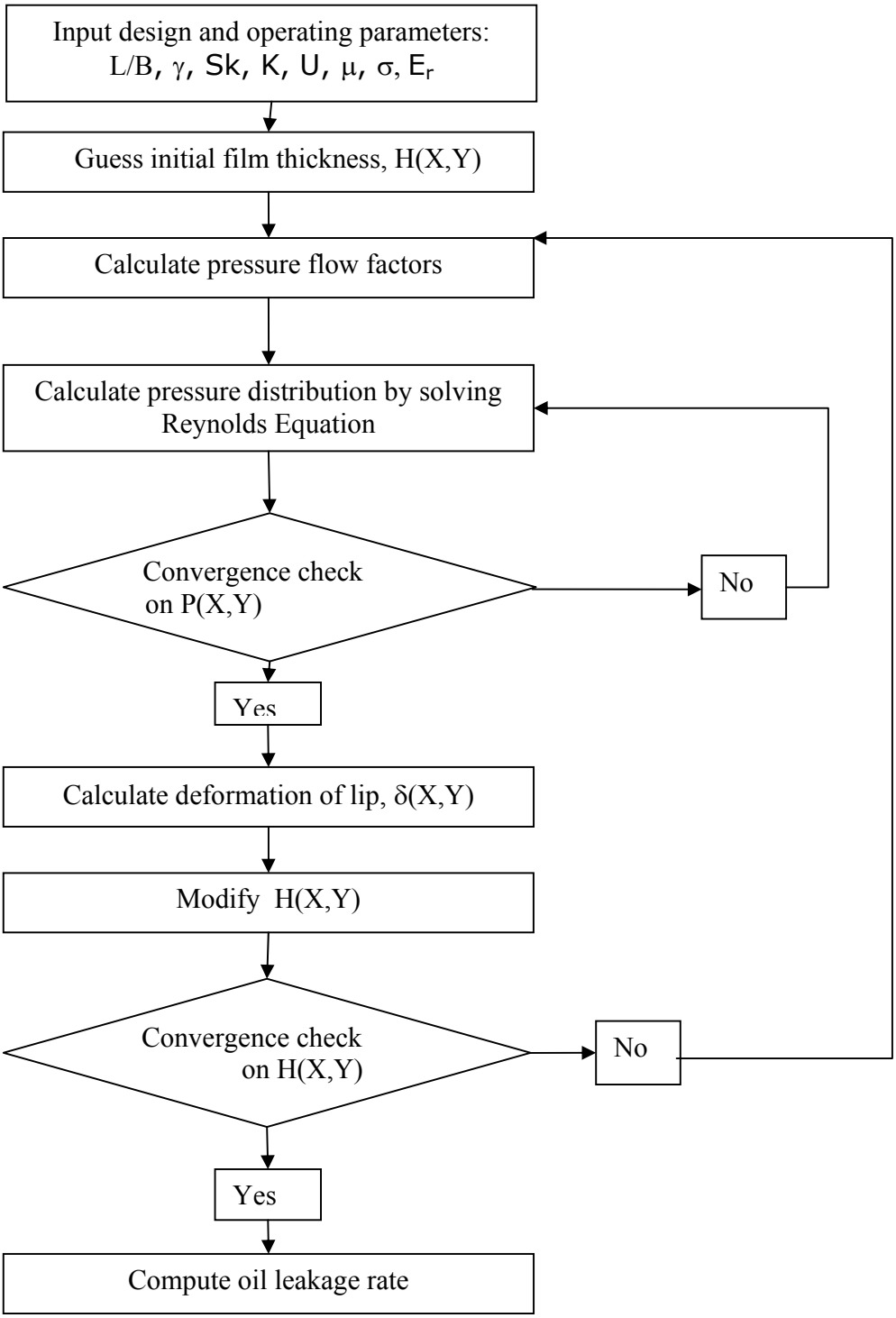

Figure 4.2 Computational Procedure

4.5 Verification of the Model

4.5.1 Inclined Bearing

As mentioned, the effect of surface roughness on the hydrodynamics of finite slider bearings operating in the partial lubrication regime is investigated by Patir and Cheng [3]. The load support is calculated by integrating the computed pressure distribution over the bearing area.

$$w = \int_0^L \int_0^B p\,dx\,dy \tag{4.10}$$

where B is the width of the bearing and L is the length of the bearing.

By using non-dimensional parameter $W = \frac{w h_m^{\,2}}{6\mu U L B^2}$, the dimensionless hydrodynamic load is given as

$$W = H_m^{\,2} \int_0^1 \int_0^1 P\,dX\,dY \tag{4.11}$$

where $H_m = \frac{h_m}{\sigma}$

In this study, the hydrodynamic pressure is calculated by using the average non-dimensional Reynolds Equation (Equation 3.3).

$$\frac{\partial}{\partial X}\left(\phi_x H^3 \frac{\partial P}{\partial X}\right) + \left(\frac{B}{L}\right)^2 \frac{\partial}{\partial Y}\left(\phi_y H^3 \frac{\partial P}{\partial Y}\right) = \frac{\partial H}{\partial X} + \frac{\partial \phi_s}{\partial X}$$

The nominal film thickness of the inclined bearing is shown in Figure 4.3 is given by:

$$h(x,y) = h_m + m(B - x)$$

where h_m is the minimum film thickness, m is the inclination (slope= tanθ) and B is the width of the bearing.

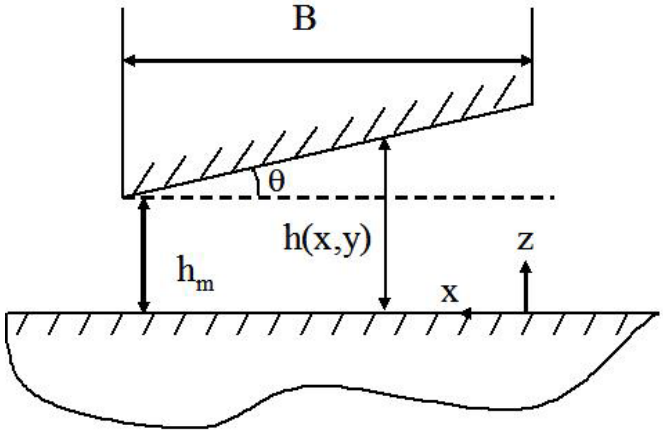

Figure 4.3 Inclined Pad Bearing Geometry

The mean pressure is zero at the boundaries of the slider

$$p(0,0) = p(L,B) = 0$$

Before solving pressure distribution, the nominal film thickness is non-dimensionalized as

$$H(X,Y) = H_m(2 - X)$$

by using the non-dimensional parameters

$$H = \frac{h}{\sigma},\ H_m = \frac{h_m}{\sigma},\ X = \frac{x}{B}$$

The non-dimensional pressure distribution is solved by the computer program developed using finite difference method. For the width-to-length ratio $\frac{L}{B} = 0.25$ and $H_m = 1$, the pressure distribution is obtained and shown in Figure 4.4.

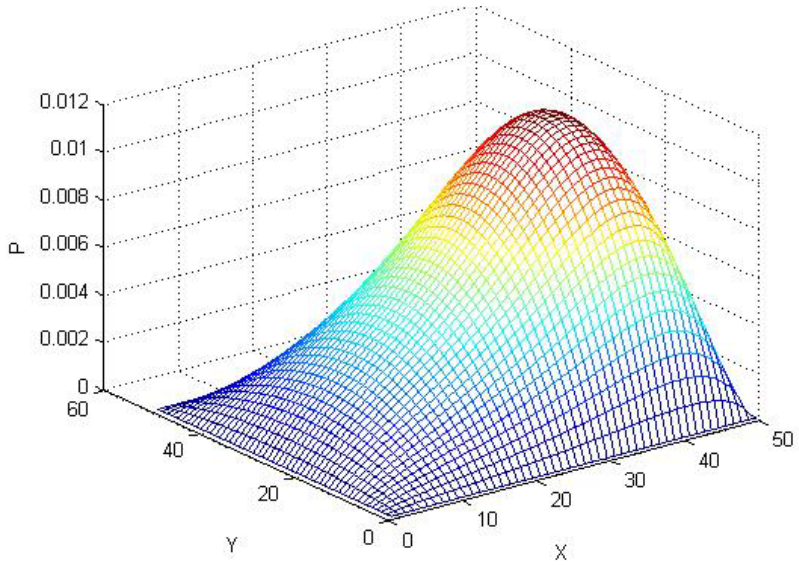

Figure 4.4 Non-dimensional pressure distribution for inclined bearing with L/B=0.25

For the width-to-length ratio L/B =0.25, the load support is calculated for different H_m and γ values by the computer program. As seen in the graph (Patir &Cheng [3]) below, the results are in agreement with the values in the paper.

Table 4.1 Non-dimensional load support values

	Hm	W		Hm	W		Hm	W
γ = 1	1	0.0025	γ = 6	1	0.0043	γ = 1/6	1	0.0012
	2	0.0018		2	0.0023		2	0.0014
	3	0.0016		3	0.0018		3	0.0014
	4	0.0015		4	0.0016		4	0.0014
	5	0.0014		5	0.0015		5	0.0014

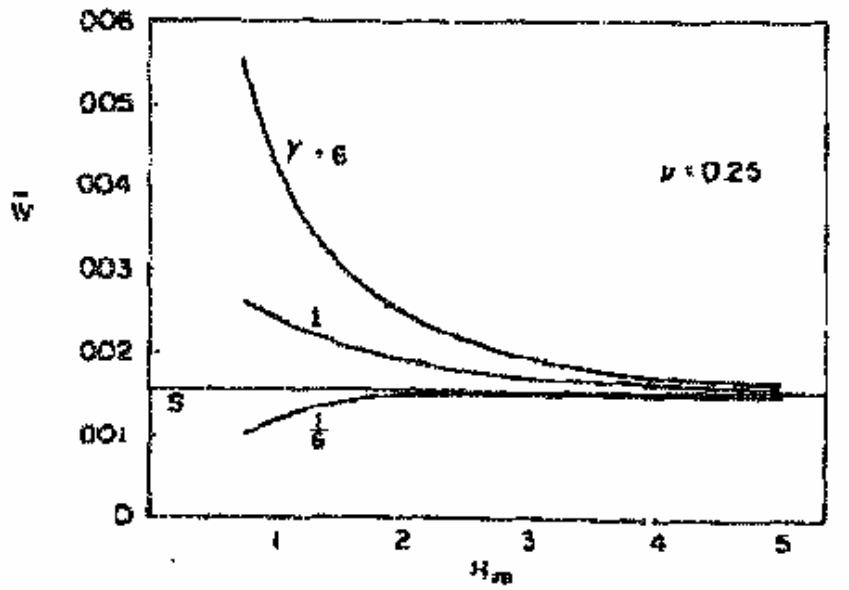

Figure 4.5 Load support for inclined pad bearing (Patir & Cheng [3])

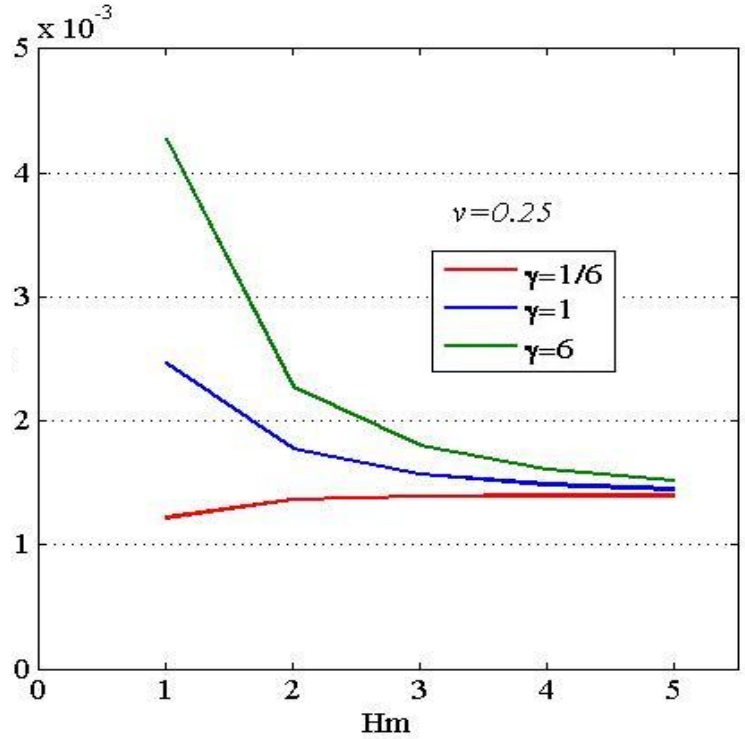

Figure 4.6 Non-dimensional load supports for inclined bearing

4.5.2 Pressure Distribution on Seal Lip

A leakage analysis on a radial lip seal (Figure 3.1) mounted on a shaft is presented by Akkok [20]. The problem defined in the study is solved for non-dimensionless leakage and results are compared with the results in the study.

Both surfaces are considered as smooth and roughness effects are not investigated. Due to the thin film thickness under the lip, the shaft radius taken as infinite and Cartesian coordinates are used to simulate contact area of the lip as seen in Figure 4.7. Under static conditions (stationary shaft), undulations on the lip surface are aligned in the axial direction. Under dynamic conditions (rotating shaft), undulations are deformed due to shear stresses in the film through the shaft rotation direction.

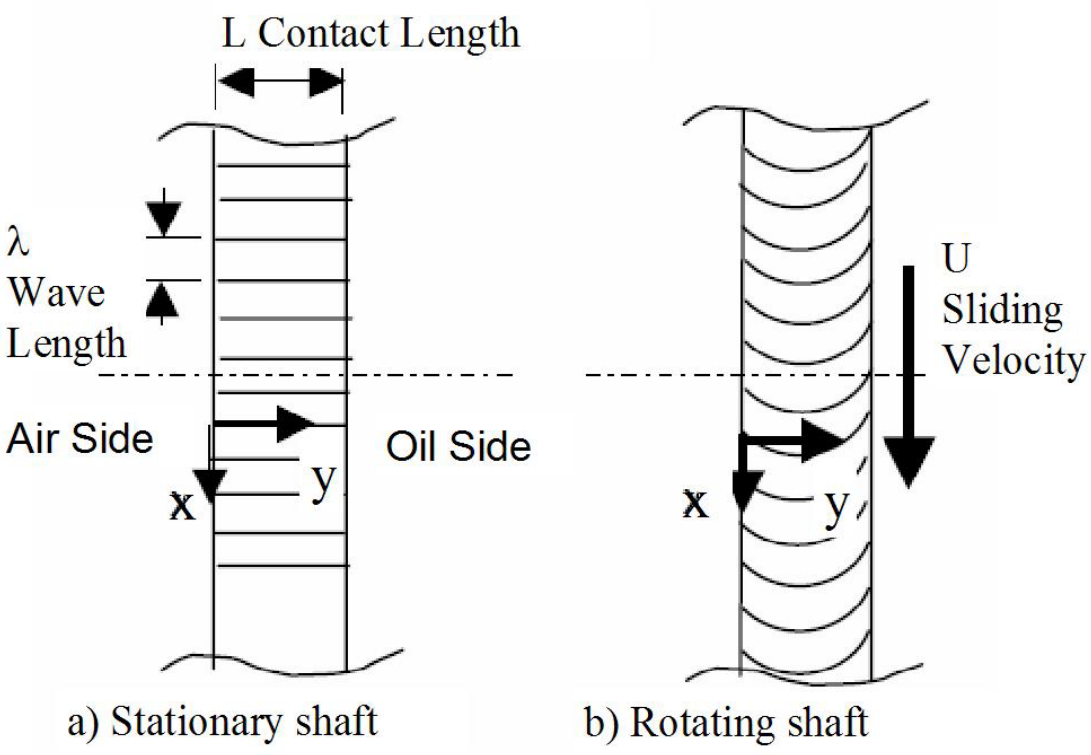

Figure 4.7 Seal lip surface undulations

The axial boundaries y=0 and y=L represent the oil and air sides of the seal, respectively. The pressure values at the air and oil side are equal to atmospheric pressure and taken as zero.

$$p(x,0) = 0\,,\ p(x,L) = 0$$

In the circumferential direction, the periodicity boundary condition is applied to contact region and wave length λ is used to solve hydrodynamic equation the boundaries x=0 and x=λ.

$$p(0,y) = p(\lambda,y)\,,\ \frac{\partial p(x=0,y)}{\partial x} = \frac{\partial p(x=\lambda,y)}{\partial x}$$

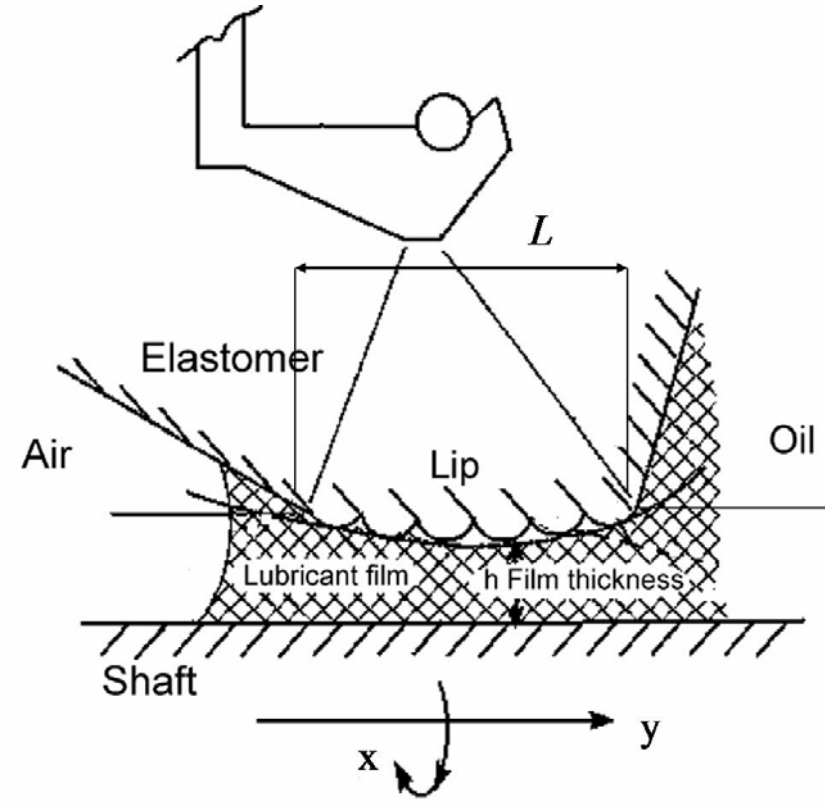

Figure 4.8 Boundary conditions for the Reynolds Equation

The Reynolds equation is solved by finite difference method. Due to the pressure distribution, the leakage through the air side in axial direction is calculated from the leakage equation (Equation 3.11) for one wave length λ. Total leakage in the axial direction for the seal can be found by multiplying the resulted flow with L/λ where L is seal circumferential length in x direction.

The radial and axial deformation of the lip is taken into account to determine the total film thickness between the lip and the shaft surface. The total film thickness H(X,Y) is defined as the sum of the average film thickness H_0, and the film thickness due to undulation of the lip, $H_r(X,Y)$, and the film thickness due to shear deformation of the lip in the sliding direction, $H_2(Y)$.

$$H(X,Y) = H_0 + H_r(X,Y) + H_2(Y) \tag{4.12}$$

where $X = \frac{x}{\lambda}$, $Y = \frac{y}{L}$

The undulation of the lip is defined as a harmonic function and due to the displacement of the lip in the circumferential direction, the film thickness can be expressed as

$$H_r(X,Y) = H_1 \cos 2\pi(X - \delta(Y)) \tag{4.13}$$

where H_1 is the non-dimensional undulation amplitude, $H_1=h_1/\sigma$ and $\delta(Y)=d(y)/\lambda$ is the non-dimensional tangential deformation of the undulation in the sliding direction which varies along the axis and can be expressed as

$$\delta(Y)=\begin{cases} D\cos\left[\dfrac{-(Y-Y_{min})}{Y_{min}}\cos^{-1}(\Delta_y)\right] & \text{for} \quad 0\le Y\le Y_{min} \\ D\cos\left[\dfrac{\pi}{2(1-Y_{min})}(Y-Y_{min})\right] & \text{for} \quad Y_{min}\le Y\le 1 \end{cases} \tag{4.14}$$

The tangential deformation of the undulation is shown in Figure 4.9.

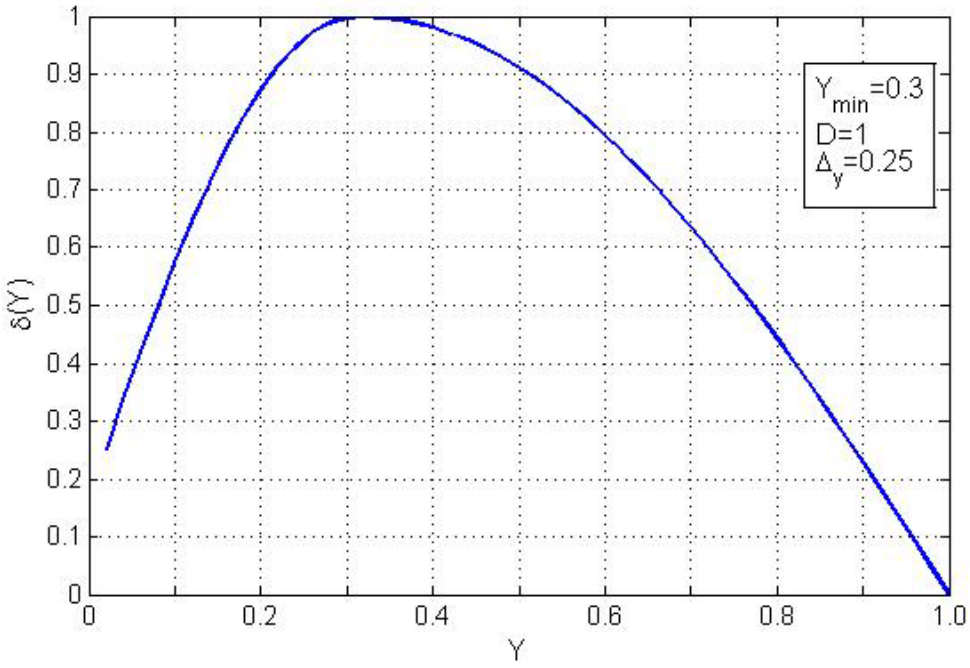

Figure 4.9 Non-dimensional tangential deformation of the undulation in the sliding direction, $\delta(Y)$ (Y_{min}=0.3, D=1, Δ_y=0.25)

where

Y_{min} : non-dimensional position of minimum film thickness

Δ_y : Tangential displacement of the oil side relative to the maximum tangential displacement

D : the ratio of maximum value of the tangential displacement to undulation period: d_{max}/λ

The variation of film thickness in the axial direction is expressed as

$$H_2(Y)=\begin{cases} H_a\left[1-\cos\left[\dfrac{\pi}{2Y_{min}}(Y-Y_{min})\right]\right] & \text{for} \quad 0\le Y\le Y_{min} \\ H_a\left[1-\cos\left[\dfrac{\pi}{2(1-Y_{min})}(Y-Y_{min})\right]\right] & \text{for} \quad Y_{min}\le Y\le 1 \end{cases} \tag{4.15}$$

where H_a is the maximum film thickness in axial direction. The variation of $H_2(Y)$ is shown in Figure 4.10.

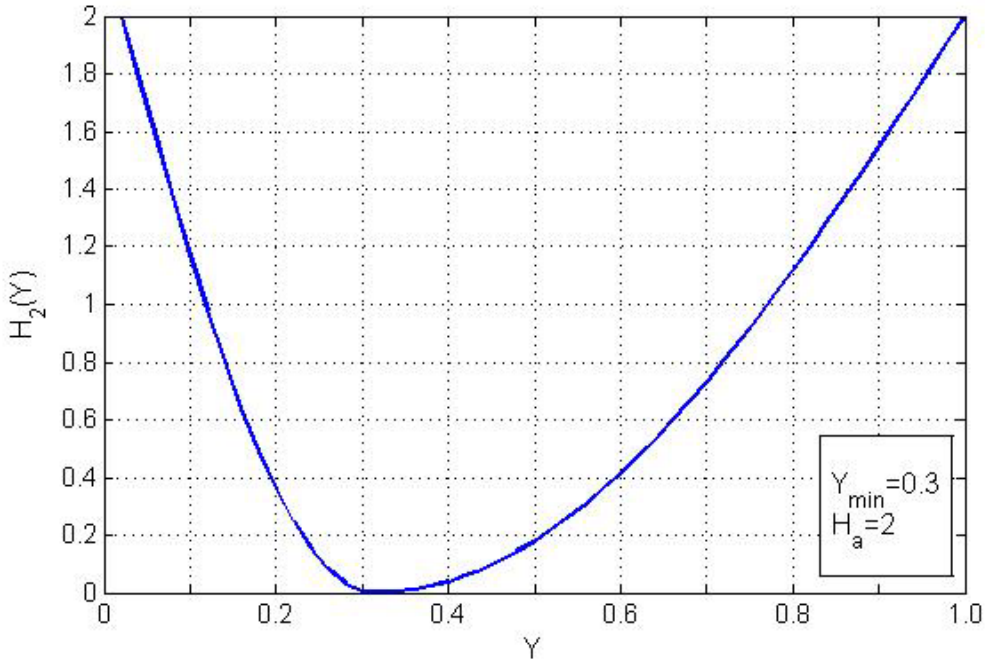

Figure 4.10 The variation of film thickness in the axial direction, $H_2(Y)$ (H_a=2, Y_{min}=0.3)

The problem is solved by the computer program for film thickness which is defined in Akkok [20]. The results are presented below. The leakage value is computed as 4.7726 which are nearly same in the problem solution in leakage analysis (Akkok [20]).

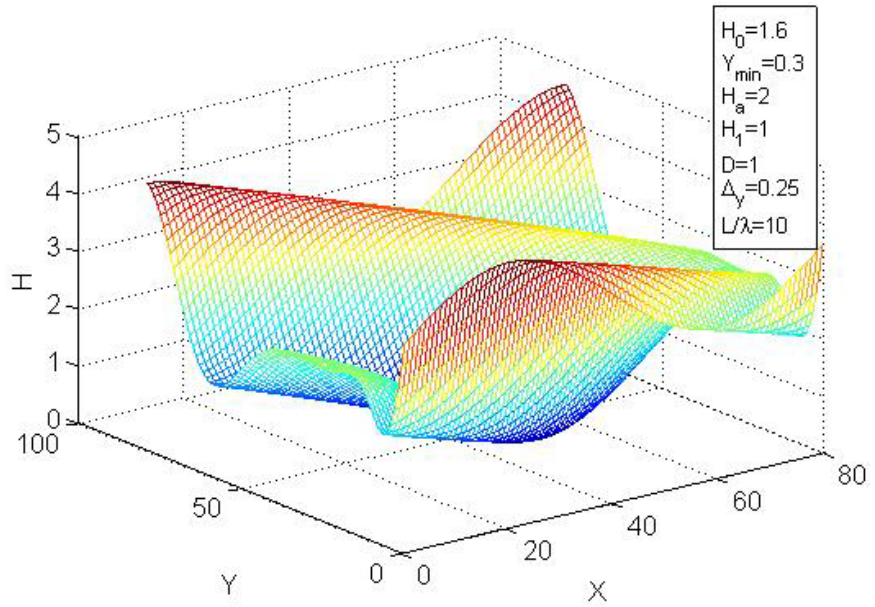

Figure 4.11 Variation of Film Thickness

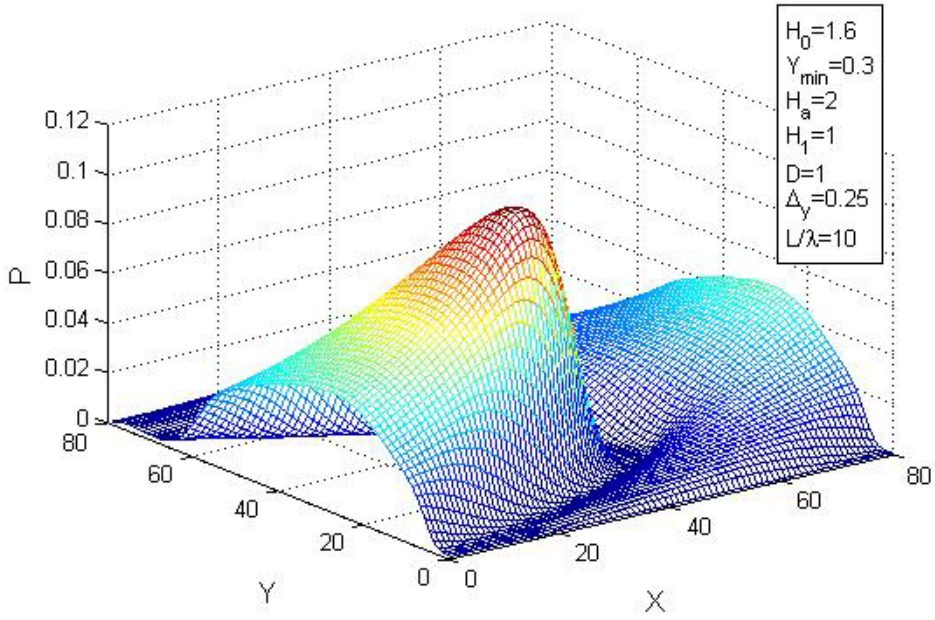

Figure 4.12 Pressure Distribution

CHAPTER 5

RESULTS AND DISCUSSION

In previous chapters, elastohydrodynamic model for lip seal leakage is presented and the method of simulation of the model is expressed. In this chapter, flow leakage analysis is performed for different case studies. Oil flow rate variation due to seal tightness for different surface roughness height distribution parameters is given. In another case study, the effect of lip seal deformation on the pressure distribution and oil film thickness is analyzed. Results and discussions are presented in following sections.

5.1 Effect of Surface Profile Height Distribution on Oil Leakage for Undeformed Seals

In the lip seal leakage simulations given in section 4.5.2, the shaft and seal surfaces are considered as smooth and roughness effects are not investigated in the solution. One step further, shaft surface roughness parameters are integrated into computations to analyze the effect of surface profile height distribution effects on oil leakage. Two parameters, namely, skewness and kurtosis, describing the surface profile height distribution are considered.

The oil film thickness is defined as in Equation 4.12. Computations are performed for a representative seal with non-dimensional base parameters of: The mean film thickness H_0=1.6, Y_{min}=0.3, Ha=2, H_1=1, D=1, Dy=0.25.

For the film thickness which is given in Figure 4.11, non-dimensional pressure distribution and oil leakage flow rate at air side is calculated by the computer program for different L/λ ratios.

Oil film pressure distributions using the flow factors given by Morales and Espejel [10] are shown in Figure 5.1 for different L/ λ ratios. As L/ λ ratio increases, the pressure values increase and give relatively higher side flow. However, for L/ λ=5 and L/ λ=10, the pressure distributions are very similar and give almost the same side flow.

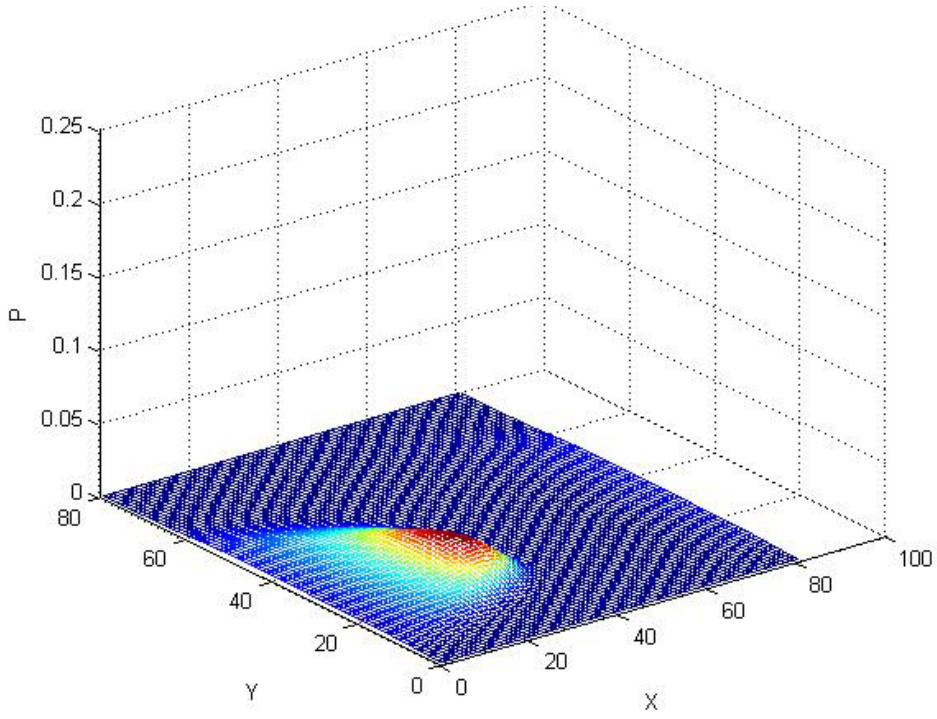

a) L/λ=0.25

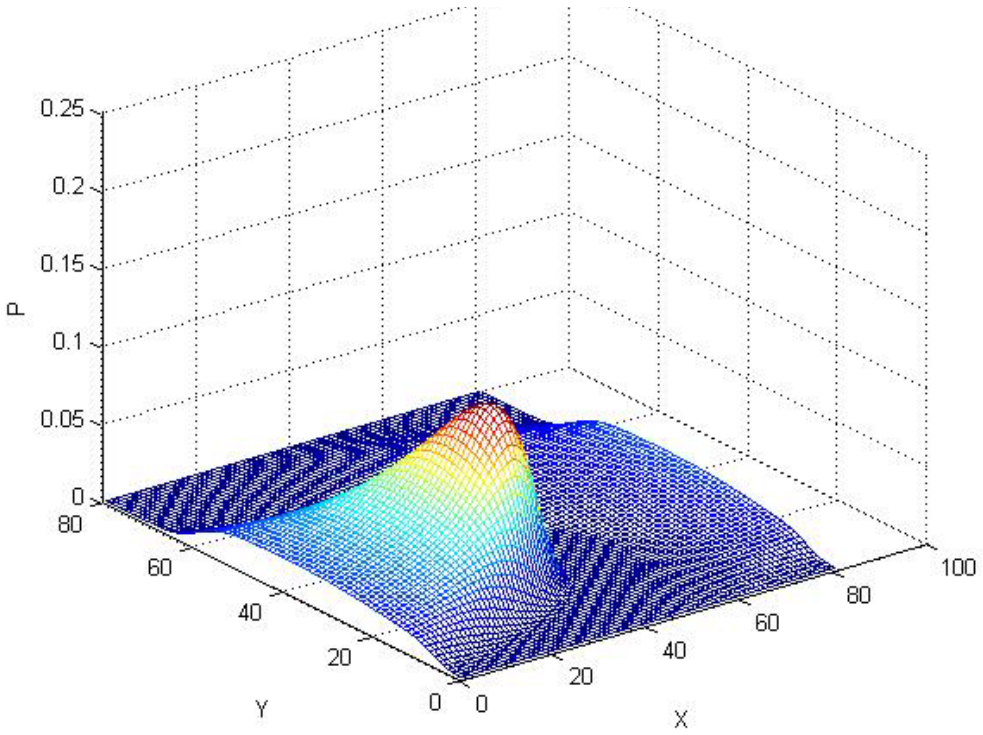
0.25
0.2
0.15
0.1
0.05
0
P
80
60
40
20
0
Y
0
20
40
60
80
100
X

b) L/ λ =1

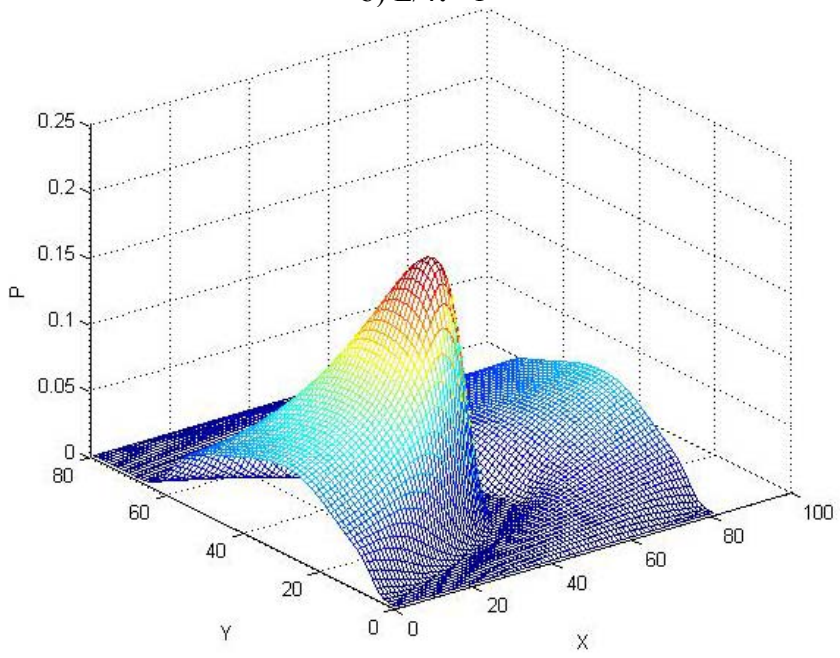
0.25
0.2
0.15
0.1
0.05
0
P
80
60
40
20
0
Y
0
20
40
60
80
100
X

c) L/λ=5

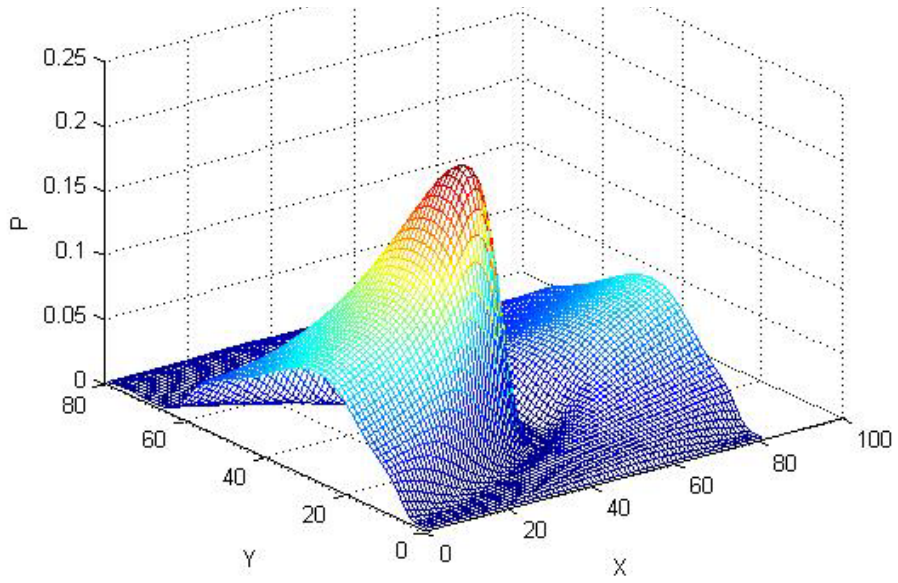

d) L/λ=10

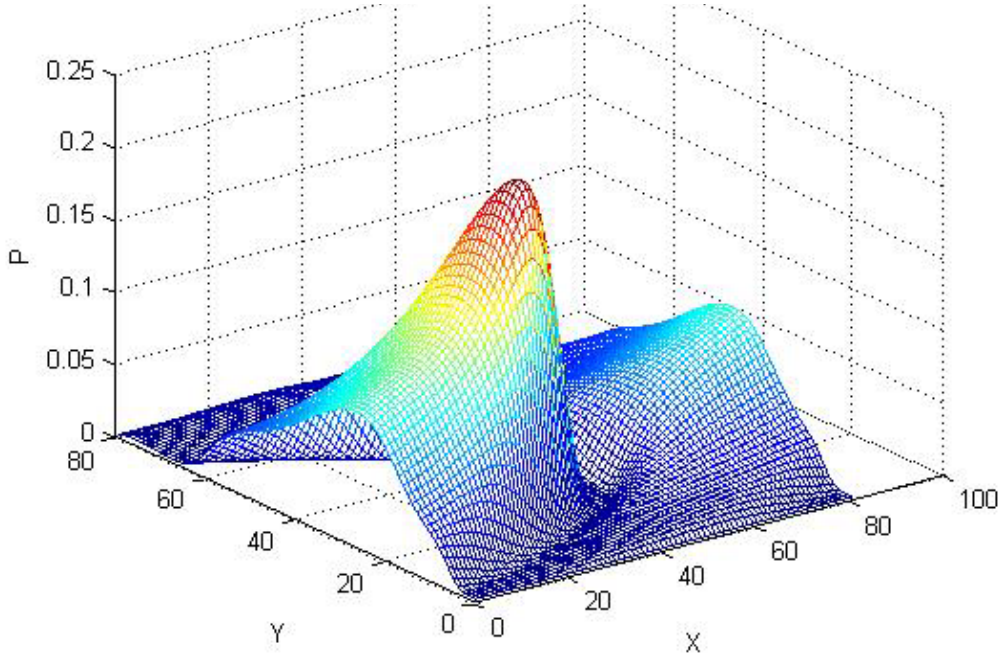

e) L/λ=16

Figure 5.1 Oil film pressure distributions for different L/λ ratios using the flow factors given by Morales and Espejel [10] (γ=1, Sk=0, K=3)

Non-dimensional oil flow rate values are shown in Figure 5.2 for different skewness and kurtosis values to investigate the effects of surface height profile distribution on side flow rate. As seen in the Figure 5.2a, for a symmetric profile (Sk=0), using different peakedness values, side flow rate through seal lip increases with kurtosis values. For same peakedness value (K=3), side flow rate through seal lip increases with skewness values as seen in Figure 5.2b.

For seal lips which have an L/λ ratio < 2, the oil leakage increases almost proportionally with the contact length (L) to width (λ) ratio. If L/λratio is about between 6 and 8, the oil leakage reaches to a peak value and for L/λ ratios higher than 10, oil flow does not change in a considerable manner.

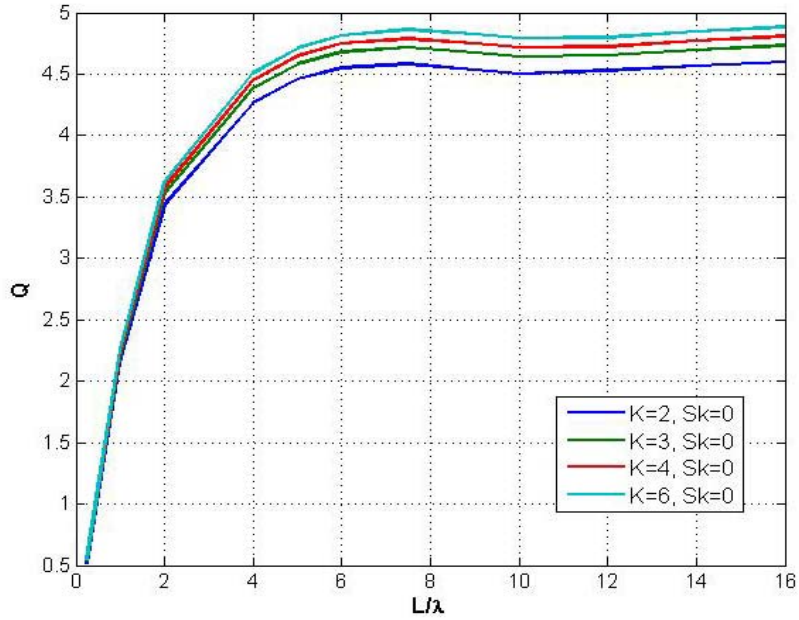

a) For different Kurtosis values, Sk=0

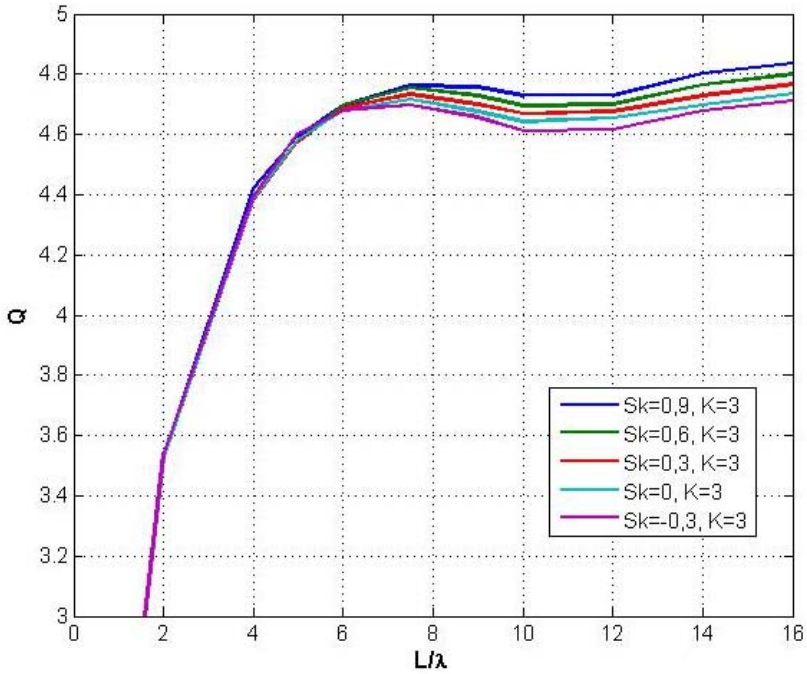

b) For different Skewness values, K=3

Figure 5.2 Variation of Non-dimensional Oil Flow rate with L/λ ratio for Different Surface profile height Distribution parameters

5.2 Simulation of Oil Leakage for Deformed Lip Seals

In sections 5.1 and 4.4.2, the seal model is used to predict oil flow rate and the effects of Gaussian and non-Gaussian flow factors on oil flow rate are investigated. However, lip deformation is not taken into consideration in these solutions.

Another model is developed to solve the flow rate for a deformed seal. In this model, the same film thickness with the examples given in sections 5.1 and 4.4.2 is used as initial film thickness. The initial film thickness and pressure distribution resulted from this film thickness are given in Figure 5.3a and 5.3b, respectively.

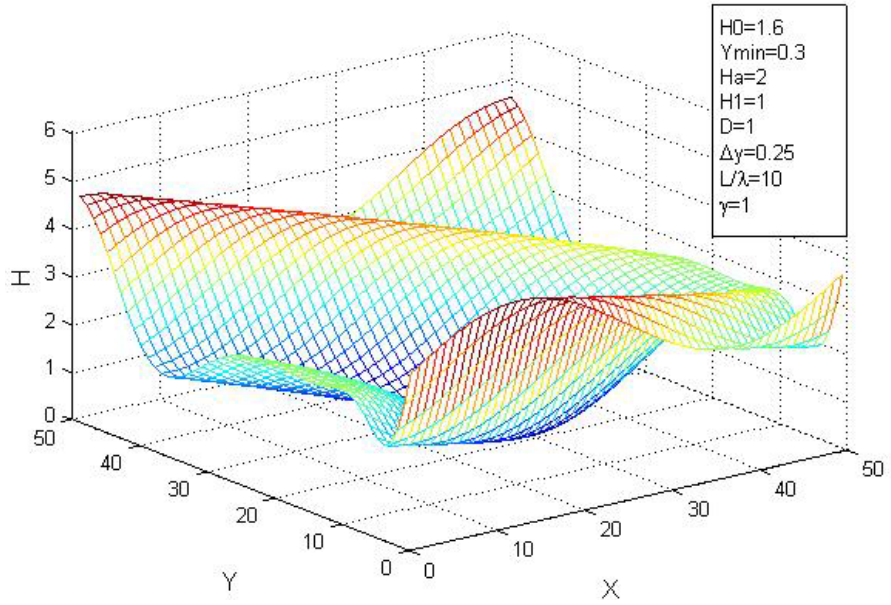

a) Initial Film Thickness

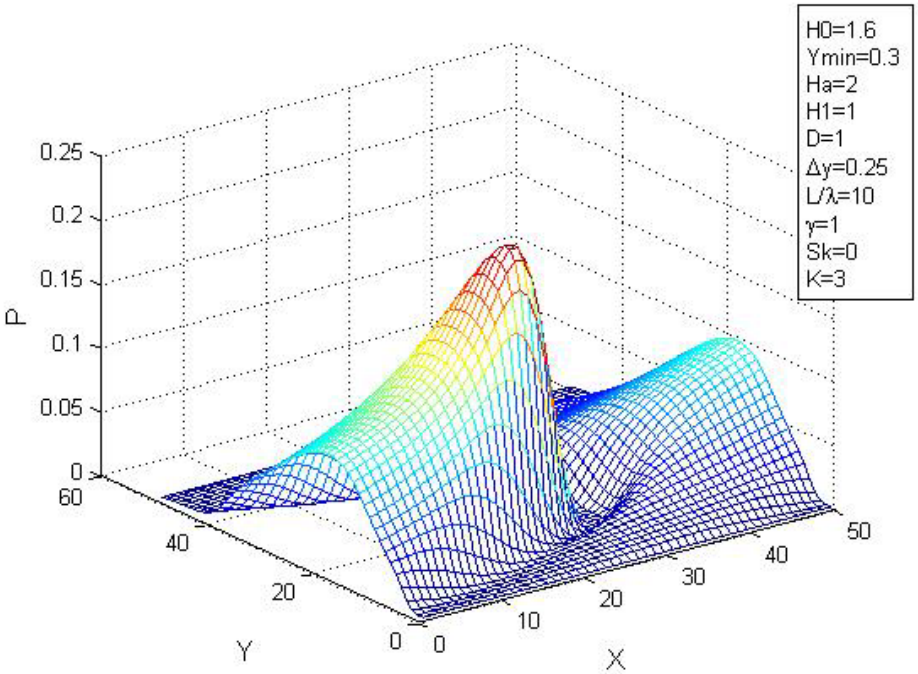

b) Pressure Distribution due to initial film thickness (undeformed lip)

Figure 5.3 Hydrodynamic solution of undeformed radial lip seal using the flow factors given by Morales and Espejel [10] (L/λ=10, γ=1, Sk=0, K=3)

Due to the initial film thickness, a pressure distribution is generated between the seal lip and the shaft. The seal lip is deformed due to the pressure distribution. The new pressure distribution is calculated by using the new film thickness. When the amount of change on the film thickness distribution is less than an acceptable value between successive iterations, the iteration process is terminated.

Computation of the lip deformation is performed with the parameter A which is calculated with base dimensional parameters of: μ=0.01 Pa-s, U=1 m/s, $\sigma=2.5\text{x}10^{-7}$ m, $\lambda=1\text{x}10^{-5}$ m, $L=1\text{x}10^{-4}$ m ($L/\lambda=10$), v_1=0.3, $E_1=207\text{x}10^{9}$ Pa, $E_2=3\text{x}10^{6}$ Pa, v_2=0.49, which gives A= 30.

The elastohydrodynamic problem is solved with the computer program developed and results are presented. The film thickness between deformed lip and shaft and the concerning pressure distribution are given in Figure 5.4a and 5.4b. As seen in the figures, the initial film thickness increases due to lip deformation and the concerning pressure distribution decreases.

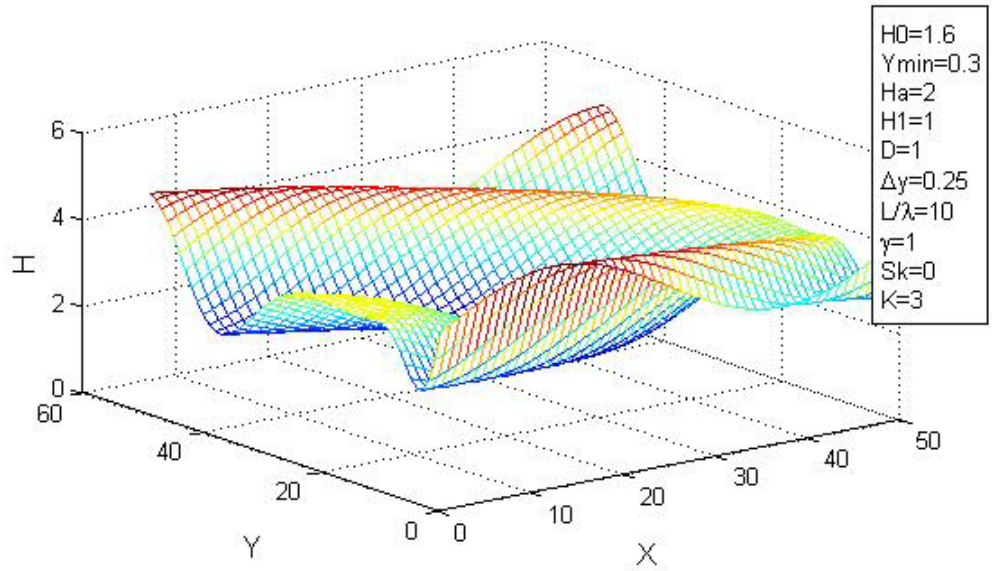

a) Film thickness due to lip deformation

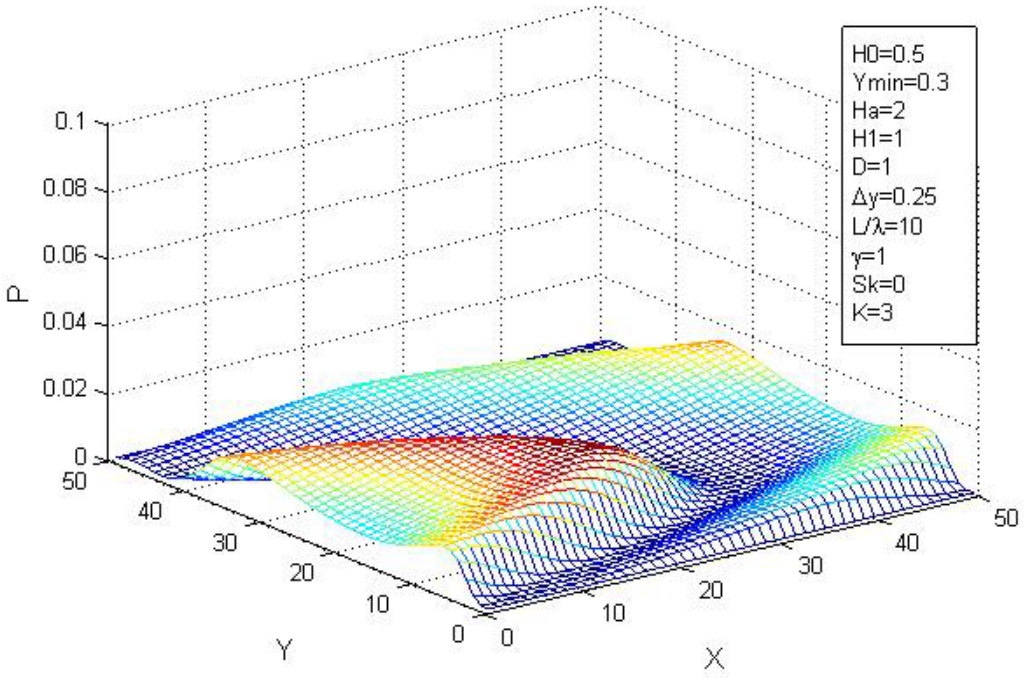

b) Pressure distribution due to deformed lip

Figure 5.4 Elastohydrodynamic solution of radial lip seal
(L/λ=10, Sk=0, γ=1, K=3, A=30)

In Figure 5.5, the distribution of the lip deformation is given. As seen in the figure, the lip deformation reaches to its highest value at the maximum pressure zone. Therefore the maximum pressure zone at initial film thickness is not observed in the deformed seal.

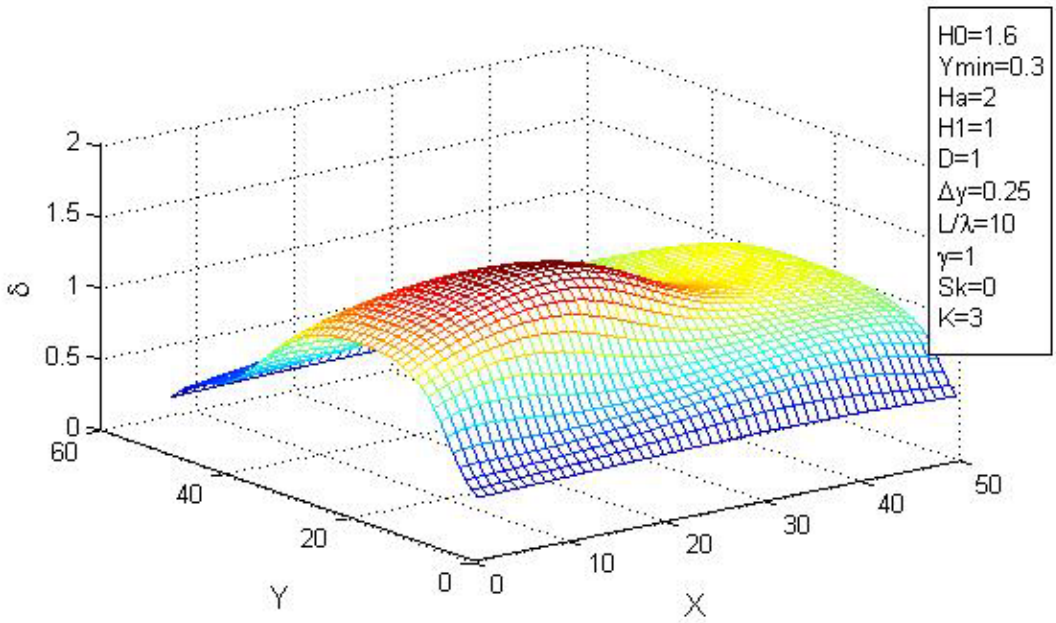

Figure 5.5 Lip deformation for radial lip seal given in Figure 5.3a (L/B=10, γ=1, Sk=0, K=3, A=30)

5.3 Effect of Initial Interference on Oil Leakage for Deformed Lip Seal

In the seal model above, there is an initial gap between seal lip and shaft surface and this gap is full of oil film. Another model is developed to solve the flow rate for a seal which is mounted on a shaft with an initial interference fit. The maximum interference value is shown with the notation δ_i in Figure 5.6.

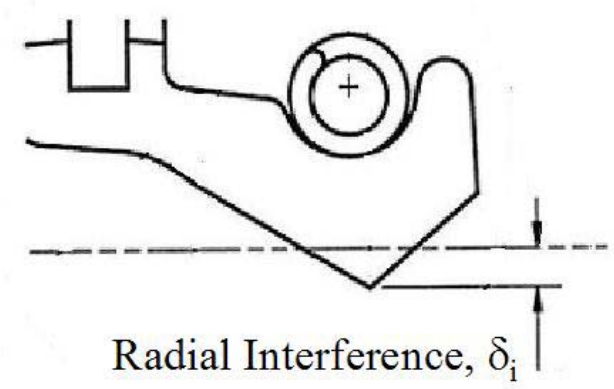

Figure 5.6 Interference between seal lip and shaft surface

In this interference fit mounted seal model, the initial film thickness is defined with an interference value by using the same equations given in the examples in section 5.1. the computations are performed for a representative seal with non-dimensional base parameters of: The mean film thickness H_0=0.5, Y_{min}=0.3, Ha=2, H_1=1, D=1, Dy=0.25, which gives δ_i=0.5. The initial film thickness is given in Figure 5.7a, and the maximum initial interference between shaft and seal lip is shown in Figure 5.7b.

The parameter A is calculated with base dimensional parameters of: μ=0.01 Pa-s, U=1 m/s, σ=2.5x10^{-7} m, λ=1x10^{-5} m, L=1x10^{-4} m (L/λ=10), ν_1=0.3, E_1=207x10^9 Pa, E_2=3x10^6 Pa, ν_2=0.49, which gives A=30.

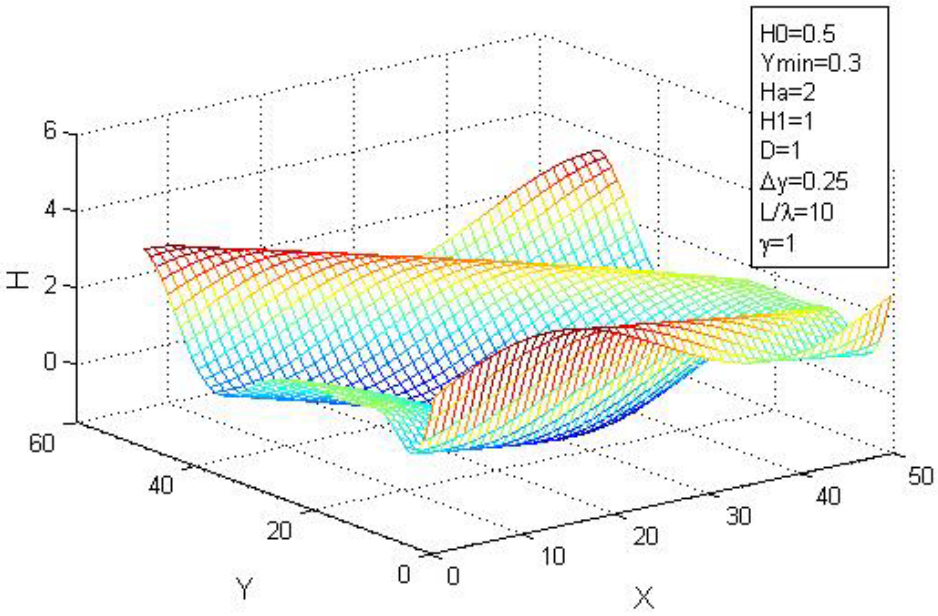

a) Initial Film Thickness

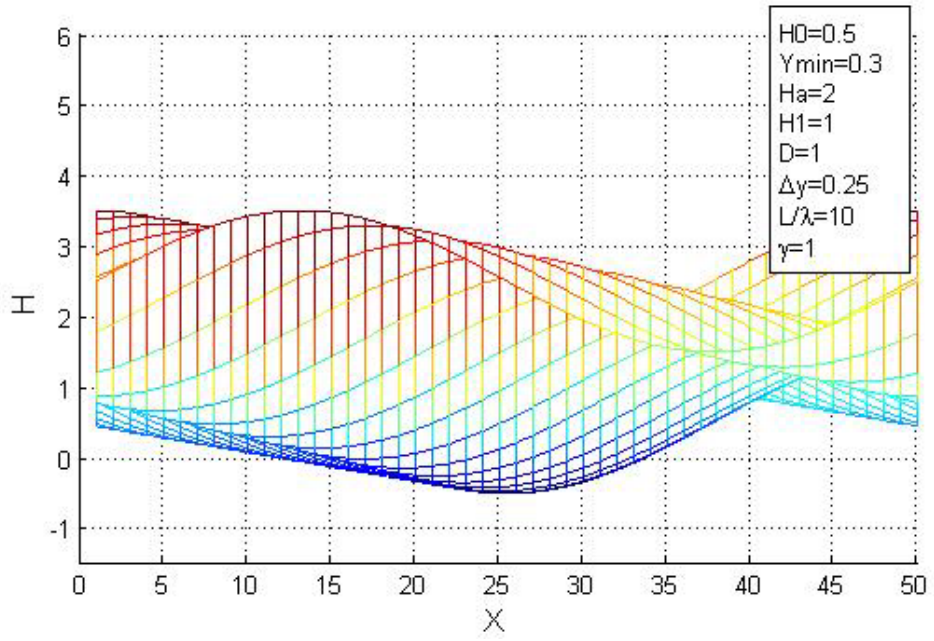

b) Initial interference between shaft surface and seal lip

Figure 5.7 Film thickness with an initial interference between radial lip seal and shaft for δ_i=0.5 (L/λ=10, γ=1, Sk=0, K=3)

Elastohydrodynamic problem is solved by the computer program developed and the results are presented. The film thickness between deformed lip and shaft and concerning pressure distribution are given in Figure 5.8a and 5.8b. As seen in the figures, the initial film thickness increases due to lip deformation and a large gap occurs between the seal lip and shaft surface. Therefore, the pressure distribution decreases to smaller values.

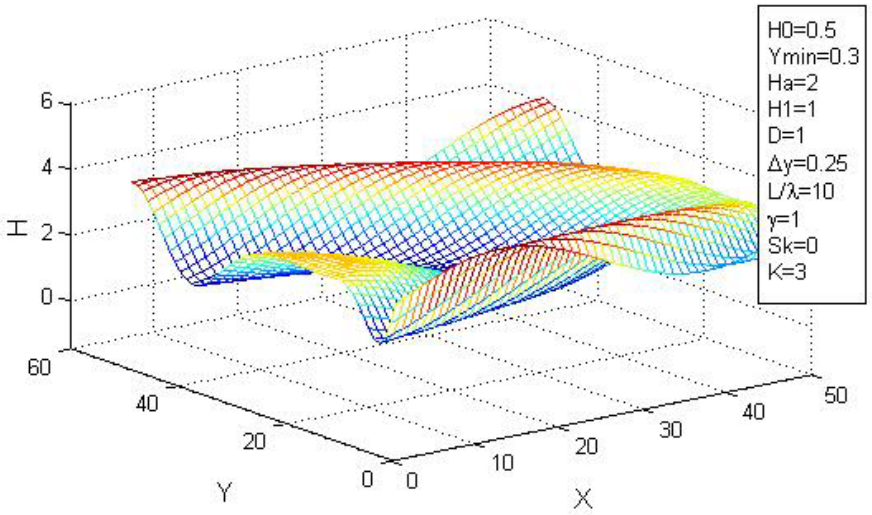

a) Film Thickness after deformation

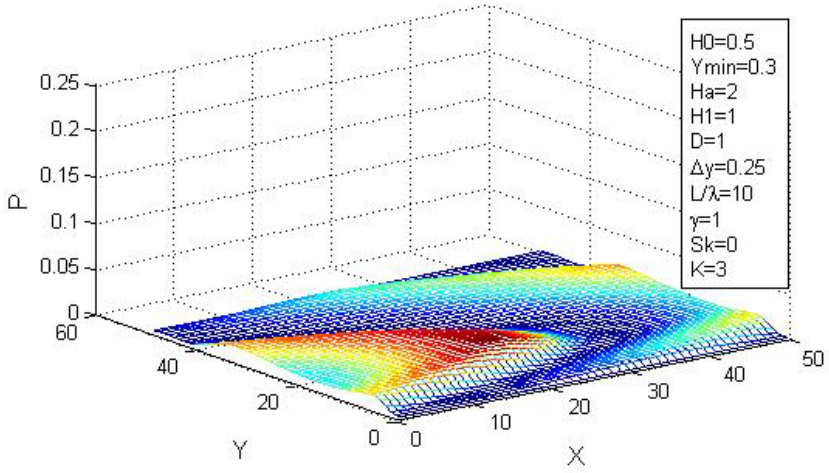

b) Pressure Distribution under deformed lip seal

Figure 5.8 Elastohydrodynamic solution of radial lip seal
(L/λ=10, Sk=0, γ=1, K=3, A=30)

In Figure 5.9, the distribution of the lip deformation is given. The maximum deflection occurs around the maximum pressure region and the minimum deflections are observed on the sides of the lip with a value of about 0.7.

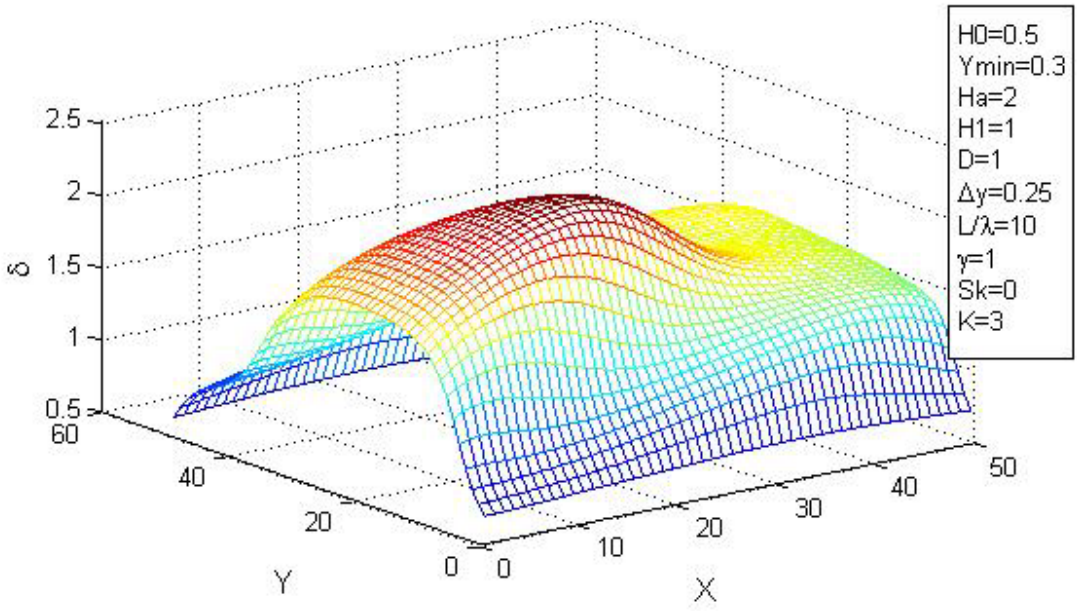

Figure 5.9 Lip deformation for radial lip seal given in Figure 5.7.a
(L/B=10, γ=1, Sk=0, K=3, A=30)

5.4 Investigation of Oil Flow Rate Variations due to Different Paramaters in Deformed Lip Seals

The computer program developed in previous chapters is used to investigate the effects of design and surface parameters on the side flow rate of a deformed seal. The results are presented in the following graphs.

In Figure 5.10, the effect of initial interference between seal lip and shaft diameter on the non-dimensional side flow rate for different A values is shown. The non-dimensional

parameter A depends on the parameters such as absolute viscosity of oil, sliding velocity, wavelength of the undulation (B=λ), shaft surface roughness and modulus of elasticity of the rubber as given in Equation 4.6 (page 45). Any variation of these parameters can affect the deflection and the oil flow rate. For same initial interference values, smaller A values give higher flow rate. As the initial interference δ_i increases, the side flow rate decreases. For smaller values of A, the side oil flow rate is nearly constant up to initial interference value of 1. No side flow rate is observed for the seal tightness higher than 1 for A=7. The side flow rate can be observed for seal tightness up to 2 for higher A values.

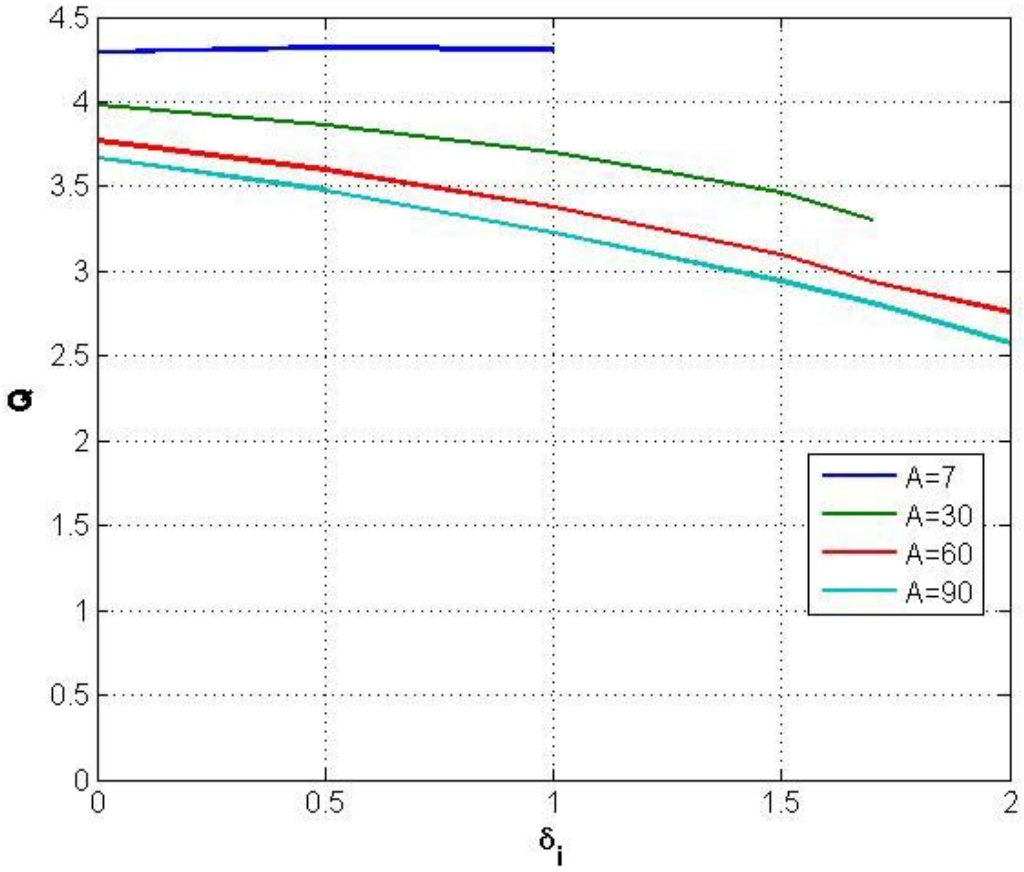

Figure 5.10 Effect of initial interference between seal lip and shaft diameter on the non-dimensional side flow rate for different A values (L/λ=10, γ=1, Sk=0, K=3)

The variation of side flow rate with L/λ ratios for three different initial seal lip tightness values is given in Figure 5.11. For L/λ < 1.8, no side oil flow is observed for all initial interference values due to no hydrodynamic pressures developed. The side flow rate increases for small interference between seal lip and shaft surface. For 1.8 < L/λ < 8, the side flow rate increases due to increase in hydrodynamic pressure with contact length (L) to undulation period (λ) ratio for all initial interference values.

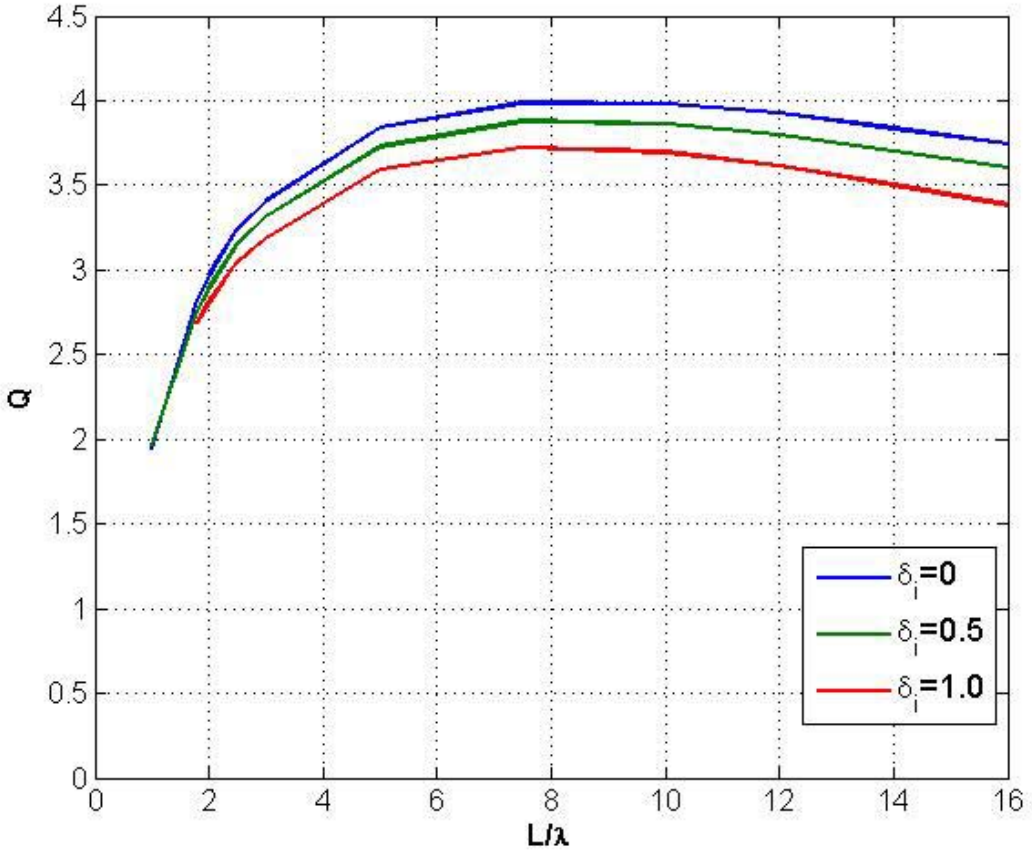

Figure 5.11 Effect of L/λ ratio on side flow rate for different initial interference values (γ=1, Sk=0, K=3, A= 30)

The effect of initial interference value of seal lip on oil flow rate is shown in Figure 5.12. For a symmetric profile (Sk=0), using different peakedness values, the side flow rate through seal lip increases with kurtosis values.

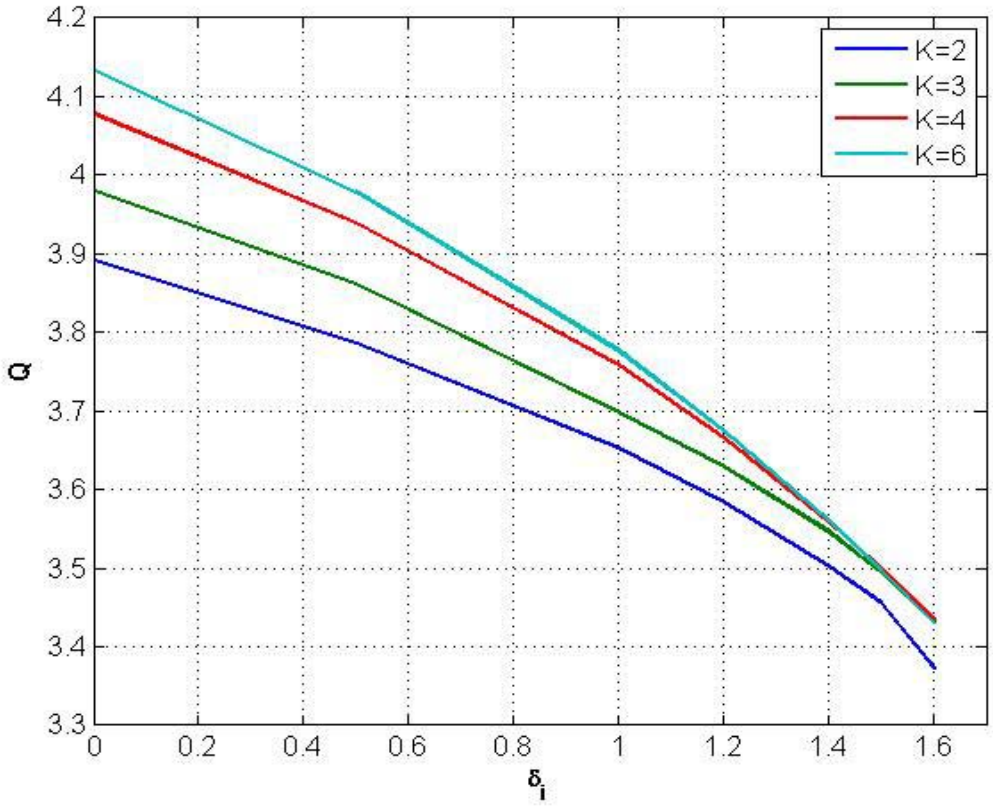

Figure 5.12 Effect of initial interference between seal lip and shaft diameter on the non-dimensional side flow rate for different kurtosis values of the surface ($L/\lambda=10$, $\gamma=1$, $A=30$, $Sk=0$)

For the same initial film geometry used, the effect of initial interference between seal lip and shaft diameter on the non-dimensional side flow rate is investigated for different Sk values and the same peakedness value (K=3) of the surface in Figure 5.13. The side flow rate decreases for all Sk values, as the initial interference increases. However, the rate of decrease in the side flow rate is higher for higher skewness values. Therefore, the side

flow rate through seal lip decreases for all skewness values up to δ=0.55 and reaches to the same value as seen in Figure 5.13. For interference values higher than 0.55, the effect of skewness becomes reversed and the side flow rate is high for lower skewness values in that case.

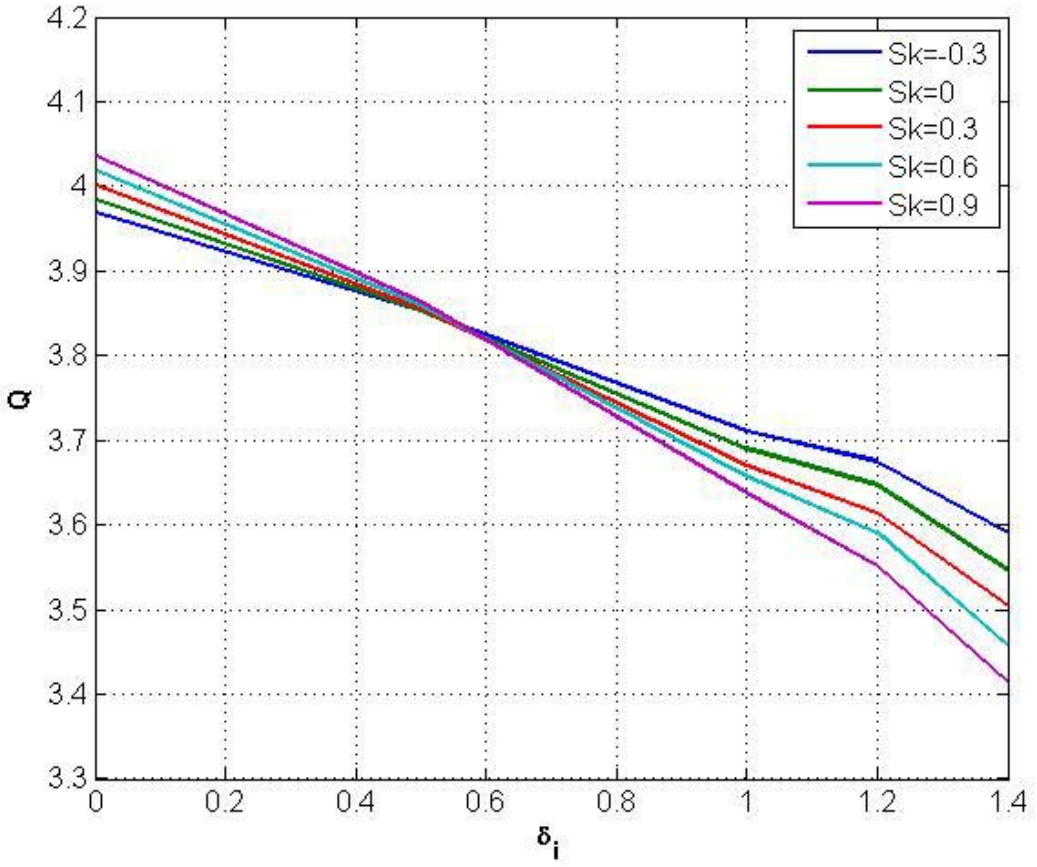

Figure 5.13 Effect of initial interference between seal lip and shaft diameter on the non-dimensional side flow rate for different Sk values of the surface
(L/λ=10, γ=1, A=30, K=3)

CHAPTER 6

CONCLUSIONS AND FUTURE WORKS

6.1 Conclusions

A computer program is developed to model and simulate elastohydrodynamic behaviors of a rotary lip seal containing undulations. Elastohydrodynamic analysis includes both the fluid mechanics of the lubricating film and the elastic deformation of the seal lip. In hydrodynamic analysis, the average Reynolds equation is solved with both Gaussian and non-Gaussian flow factors to investigate the effect of surface roughness. The effects of skewness and kurtosis parameters of the surface roughness height distribution on hydrodynamic pressure are taken into consideration by using modified flow factors.

It was found that the side oil flow rate can be predicted for a lip seal containing undulations.

Initial tightness of the seal mounted on a shaft is also investigated to analyze its effect on side flow rate of oil. The deflection parameter A depends on the parameters such as absolute viscosity of oil, sliding velocity, wavelength of the undulation ($B=\lambda$), shaft surface roughness and modulus of elasticity of the rubber. The amount of deflection and concerning oil flow rate are sensitive to any variation of these parameters.

- A radial lip seal is usually mounted on a shaft with an initial interference. In operating conditions, seal lip deforms and oil film fills the gap between seal and shaft generating a pressure distribution. For small deformation parameters such as A=7 and the maximum initial interference value δ_i>1, the hydrodynamic pressure developed is not sufficient to deform the rubber lip to form a fluid film between the shaft surface and the seal lip. Therefore, full contact occurs between seal lip and shaft surface and no oil flow is observed in that case.

- For the same initial interference values, smaller A values give higher side flow rate values. For higher initial interference δ_i, the side flow rate decreases. For smaller values of A, the side flow rate is nearly constant up to initial interference value of 1. No flow rate is observed for seal tightness higher than 1 for A=7. For higher A values, the side flow rate can be observed for the maximum initial seal tightness up to 2.

- The side flow rate slightly decreases with increase in initial seal tightness for the same surface roughness parameters.

- For the same length to undulation width ratio (L/λ), the side flow rate decreases with initial interference between seal lip and shaft surface. For $L/\lambda < 1.8$ and A=30, no side oil flow is observed for all initial interference values due to no hydrodynamic film developed. For $1.8 < L/\lambda < 8$, the side flow rate increases due to increase in pressure with contact length (L) to undulation period (λ) ratio. For $L/\lambda > 8$, it decreases slightly.

- For a symmetric profile height distribution (Sk=0), the side flow rate through seal lip is observed to increase with kurtosis values.

- For higher initial interference values, the side flow rate decreases for all Sk values. However, the rate of decrease in the side flow rate is higher for higher skewness values. Therefore, the side flow rate through seal lip decreases for all skewness values up to about δ_i=0.55 and reaches to the same value. For the initial interference values higher than 0.55, the effect of skewness becomes reversed and the side flow rate is high for lower skewness values in that case.

6.2 Future Works

It is vital to note that all the conclusions listed are restricted with the assumptions considered when the model is developed such as incompressible and Newtonian fluid film, isothermal bounding surfaces, no convective heat transfer through thin oil film, etc. In the program, surface roughness effects are investigated using Gaussian and non-Gaussian flow factors. These factors are found in references Patir and Cheng [3] factors as Gaussian flow factors and Espejel [10] as non-Gaussian flow factors. All these factors are derived from statistical analysis.

The computer program can be improved as a future work by adding new features to improve the modeling of oil leakage in lip seals:

- The simulations can also be conducted by using different softwares to compare the results.
- As an improvement, a module can be added to the computer program to derive the flow factors according to measured values of surface parameters using statistical methods.
- The flow coefficients can be improved for small values of the mean film thickness between rough surfaces.

- Since the contact region is very small in size, frictional heating can affect the hydrodynamic flow. Therefore thermohydrodynamic analysis can be studied to take into account the frictional heating especially for seals mounted with initial interference.
- The initial undulation shape and the tangential displacement of the undulations due to shear can affect the leakage in the axial direction. Therefore, the radial and tangential deformation of the seal is to be considered in the hydrodynamic analysis.
- In this study, elastohydrodynamic analysis of a radial lip seal containing undulations is performed. Other seal models can be improved to investigate the effects of seal design parameters such as undulation amplitude, undulation period, the slope of the seal on the oil and air sides, flex section thickness, seal contact length, etc. on side flow rate. Also, radial load and spring characteristics for a particular shaft diameter can be analyzed by improving a parametrical seal model.

REFERENCES

[1] Baart P, Lugt P, Prakash B., 2009, "Review of the lubrication, sealing, and pumping mechanisms in oil- and grease-lubricated radial lip seals", Proceedings of the Institution of Mechanical Engineers, Part J, Journal of Engineering Tribology, Vol. 223(3), pp. 347-358.

[2] Johnston D.E., 1999, "Design aspects of modern rotary shaft seals" , Proc. I.Mech.E., Vol. 213, Part J, pp. 203-213.

[3] Patir, N. and Cheng, H. S., 1979, "Application of average flow model to lubrication between rough sliding surfaces", J. Lubric. Technol., Vol. 101, pp. 220–229.

[4] Harp, S. R., and Salant, R. F., 2001, "An average flow model of rough surface lubrication with inter-asperity cavitation,'' ASME J. Tribol., Vol. 123, pp. 134–143.

[5] Lo, S-W, 1992, "On the effects of roughness orientation – a mapping and double scale analysis of flow factors," ASME J. of Tribology, Vol. 114, pp. 747-754.

[6] Salant, R. F. and Rocke, A.H., 2004, "Hydrodynamic analysis of the flow in a rotary lip seal using flow factors", ASME J Tribol., Vol. 126, pp. 156–161.

[7] Letalleur, N., Plouraboue', F. and Prat, M., 2002, "Average flow model of rough surfaces lubrication: Flow factors for sinusoidal surfaces", J. Tribology., Vol. 124, pp. 539-546.

[8] Prat, M., Plouraboue', F. and Letalleur, N., 2002, "Averaged Reynolds equation for flow between rough surfaces in sliding motion", J. Trans. Por. Med., Vol. 48, pp. 291-313.

[9] Hajjam, M., Bonneau, D., 2006, "Influence of the roughness model on the thermoelastohydrodynamic performances of lip seals", Tribology International, Vol. 39, pp. 198–205.

[10] Morales-Espejel G. E., 2009, “Flow factors for non-Gaussian roughness in hydrodynamic lubrication: an analytical interpolation”, Proc. IMechE, Vol. 223 Part C: J. Mechanical Engineering Science, pp. 1433-1441.

[11] Peeken, H. J., Knoll, G., Rienäcker, A., Lang, J., and Schönen, R., 1997, “On the numerical determination of flow factors”, ASME, J. Tribol., Vol. 119, pp. 259–264.

[12] Maoui A., Hajjam M., Bonneau D., 2008, “Effect of 3D lip deformations on elastohydrodynamic lip seals behaviour”, Tribology International, Vol. 41, pp. 901-907

[13] Salant, R. F., 1997, “Modeling rotary lip seals”, Wear, Vol. 207, pp. 92-99.

[14] Thatte, A. and Salant, R. F., 2009, "Transient EHL Analysis of an elastomeric hydraulic seal", J. Tribology”, Vol. 42, pp. 1424–1432.

[15] Kasem, A., 2006, “Numerical analysis of leakage rate for the selection of elastomeric sealing materials”, Sealing Technology, pp. 7–11.

[16] Salant, R. F., Flaherty, A. L., 1994, “Elastohydrodynamic analysis of reverse pumping in rotary lip seals with microundulations”, Jour. of Tribology, Vol. 116, pp. 56-62.

[17] Yang An-Shik, Wen Chih-Yung, Chun-ShiangTseng, 2009, “Analysis of flow field around a ribbed helix lip seal”, Tribology International, Vol. 42, pp. 649–656.

[18] Lebeck A. O., 1999, “Mixed lubrication in mechanical face seals with plain faces”, Proc Instn Mech Engrs, Vol. 213, pp. 163-175.

[19] Gohar, R., “Elastohydrodynamics”, Ellis Horwood, Chichester, England, 1988.

[20] Akkok, M., 2001, “Leakage Analysis in Lip Seals, Proceedings of II. National Hydraulics and Pneumatics Congress and Exhibition, E/2001/278-1:301-309 (in Turkish)

APPENDIX A

PROGRAM CODE

```
H0=1.9;
Ht=-0.4;
H1=1;
Ymin=0.3;
Ha=2;
D=1;
Dy=0.25;
LD=10;

n=0.01; %Pa-s
U=1;    %m/s
sigma=2.5*10^-7; %m
B=1*10^-5; %m
L=B*LD; %m

v1=0.3; %poison's ratio
E1=207*10^9; %Pa
E2=3*10^6; %Pa
v2=0.49;
Er=1/(1/pi*((1-v1^2)/E1+(1-v2^2)/E2));%MPa

DEFACTOR=(6*n*U*B^2)/Er/(sigma^3);

RFp=1.95;   %RF value for pressure iteration
RFd=0.5; %RF value for deformation iteration
pc=0;

M=50;
N=50;

dx=1/(N-1);
dy=1/(M-1);

%INITIAL DEFORMATION s=0

for j=1:M;
    for i=1:N;
        s(j,i)=0;
        sold=s;
    end
end
```

```
 %REAL FILM THICKNESS H(j,i)=H0+Hr(j,i)+H2(j,i);

for j=1:M;
    for i=1:N;

        xi=(i-1)*dx;
        yj=(j-1)*dy;

             % computation of Hr

         if (yj<=Ymin)

            del(j,i)=D*cos(-(yj-Ymin)*acos(Dy)/Ymin);

        else
            del(j,i)=D*cos(pi*(yj-Ymin)/(2*(1-Ymin)));

        end

        Hr(j,i)=cos(2*pi*(xi-del(j,i)));

        % computation of H2

         if (yj<=Ymin)

            H2(j,i)=Ha*(1-cos(pi*(yj-Ymin)/(2*Ymin)));

        else
            H2(j,i)=Ha*(1-cos(pi*(yj-Ymin)/(2*(1-Ymin))));

        end

        Hreal(j,i)=Ht+Hr(j,i)+H2(j,i);

    end

end

%INITIAL FILM THICKNESS H(j,i)=H0+Hr(j,i)+H2(j,i);

for j=1:M;
    for i=1:N;

        xi=(i-1)*dx;
        yj=(j-1)*dy;
```

```
         % computation of Hr

         if (yj<=Ymin)

            del(j,i)=D*cos(-(yj-Ymin)*acos(Dy)/Ymin);

        else
            del(j,i)=D*cos(pi*(yj-Ymin)/(2*(1-Ymin)));

        end

        Hr(j,i)=cos(2*pi*(xi-del(j,i)));

        % computation of H2

        if (yj<=Ymin)

            H2(j,i)=Ha*(1-cos(pi*(yj-Ymin)/(2*Ymin)));

        else
            H2(j,i)=Ha*(1-cos(pi*(yj-Ymin)/(2*(1-Ymin))));

        end

        Hi(j,i)=H0+Hr(j,i)+H2(j,i);

    end

end

figure
mesh(Hi)

iterationnumber=0;  %iteration value for deformation

for t=1:100;

    if t<=1
        RFp=1.98;

    else
        RFp=1.9;
    end

xss=0;
rss=0;
```

```
for j=1:M;
    for i=1:N;

   % computation of H

        %PREVIOUS ITERATION RESULT FOR LIP DEFORMATION CALLED sold

        sold=s;

         if min(min(Hreal))<=0.5

         H(j,i)=Hi(j,i);

          else

         H(j,i)=Hreal(j,i);

          end

          Hold(j,i)=H(j,i);

    end

end

%MODIFIED FLOW FACTORS

for j=1:M;
    for i=1:N;

        xi=(i-1)*dx;
        yj=(j-1)*dy;

        h(j,i)=H(j,i);

        if min(min(H))>0.5

%MODIFIED FLOW FACTORS

        Sk=0.9;
        K=3;

        h(j,i)=H(j,i);

        fx(j,i)=1-0.9*exp(-0.56*h(j,i))+((1/h(j,i))^3)*Sk;
        dfx(j,i)=63/125*exp(-14/25*h(j,i))-(3/(h(j,i)^4))*Sk;
```

```
        fy(j,i)=1-0.9*exp(-0.56*h(j,i))+((1/h(j,i))^3)*Sk;

        dfy(j,i)=63/125*exp(-14/25*h(j,i))-(3/(h(j,i)^4))*Sk;

gama=1;
g1(j,i)=-3*(1/H(j,i))-30*(1/H(j,i))^3;
g2(j,i)=1+6*(1/H(j,i))^2+450*(gama)*(1/H(j,i))^4;

Ng1(j,i)=6*Sk*(1/H(j,i))^2-10*(K-3)*(1/H(j,i))^3;
Ng2(j,i)=-10*Sk*(1/H(j,i))^3+150*(gama)*(K-3)*(1/H(j,i))^4;
dfs(j,i)=93051/50000/H(j,i)^(1/50)*exp(-
23/25*H(j,i)+1/20*H(j,i)^2)*(1+(6*Sk/H(j,i)^2-(10*K-30)/H(j,i)^3)/(-
3/H(j,i)-30/H(j,i)^3))/(1+(-10/H(j,i)^3*Sk+150*gama*(K-
3)/H(j,i)^4)/(1+6/H(j,i)^2+450*gama/H(j,i)^4))+1899/1000*H(j,i)^(49/50)
*(-23/25+1/10*H(j,i))*exp(-
23/25*H(j,i)+1/20*H(j,i)^2)*(1+(6*Sk/H(j,i)^2-(10*K-30)/H(j,i)^3)/(-
3/H(j,i)-30/H(j,i)^3))/(1+(-10/H(j,i)^3*Sk+150*gama*(K-
3)/H(j,i)^4)/(1+6/H(j,i)^2+450*gama/H(j,i)^4))+1899/1000*H(j,i)^(49/50)
*exp(-23/25*H(j,i)+1/20*H(j,i)^2)*((-12/H(j,i)^3*Sk+3*(10*K-
30)/H(j,i)^4)/(-3/H(j,i)-30/H(j,i)^3)-(6*Sk/H(j,i)^2-(10*K-
30)/H(j,i)^3)/(-3/H(j,i)-30/H(j,i)^3)^2*(3/H(j,i)^2+90/H(j,i)^4))/(1+(-
10/H(j,i)^3*Sk+150*gama*(K-
3)/H(j,i)^4)/(1+6/H(j,i)^2+450*gama/H(j,i)^4))-
1899/1000*H(j,i)^(49/50)*exp(-
23/25*H(j,i)+1/20*H(j,i)^2)*(1+(6*Sk/H(j,i)^2-(10*K-30)/H(j,i)^3)/(-
3/H(j,i)-30/H(j,i)^3))/(1+(-10/H(j,i)^3*Sk+150*gama*(K-
3)/H(j,i)^4)/(1+6/H(j,i)^2+450*gama/H(j,i)^4))^2*((30/H(j,i)^4*Sk-
600*gama*(K-3)/H(j,i)^5)/(1+6/H(j,i)^2+450*gama/H(j,i)^4)-(-
10/H(j,i)^3*Sk+150*gama*(K-
3)/H(j,i)^4)/(1+6/H(j,i)^2+450*gama/H(j,i)^4)^2*(-12/H(j,i)^3-
1800*gama/H(j,i)^5));

  else
%         roughness effect deactivation
        dfs(j,i)=0;
        dfx(j,i)=0;
        dfy(j,i)=0;
        fx(j,i)=1;
        fy(j,i)=1;

        end

    end
end

for j=1:M;
    for i=1:N;
```

```
        p(j,i)=0;

    end

end

piteration=0;

for j=1:M;
    for i=1:N;

        dd(j,i)=fx(j,i)/dx^2+fy(j,i)/((LD*dy)^2);

        A(j,i)=2*dd(j,i);

    end
end

for j=2:M-1;
    for i=2:N-1;

        DHX(j,i)=(H(j,i+1)-H(j,i-1))/(2*dx);

        DHY(j,i)=(H(j+1,i)-H(j-1,i))/(2*dy);

    end
end

for k=1:500;

xs=0;
rs=0;

for i=2:N-1;
    for j=2:M-1;

        z=p(j,i);

        ds=((3*fx(j,i)/H(j,i)+dfx(j,i))*(p(j,i+1)-p(j,i-1))/(2*dx)-
((1+dfs(j,i))/H(j,i)^3));

        d=fx(j,i)*(p(j,i+1)+p(j,i-1))/(dx^2)+ds*DHX(j,i);

        b=(fy(j,i)/LD^2)*(p(j+1,i)+p(j-1,i))/(dy^2)+(p(j+1,i)-p(j-
1,i))/((2*dy*LD^2))*(3*fy(j,i)/H(j,i)+dfy(j,i))*DHY(j,i);

        p(j,i)=z+RFp*((d+b)/A(j,i)-z);
```

```
        if p(j,i)>=0

            p(j,i)=p(j,i);
                else
                       p(j,i)=pc;
          end

       xs=xs+abs(p(j,i));

       rs=rs+abs(p(j,i)-z);
    end

    for j=1:M

        p(j,1)=p(j,N-1);
        p(j,N)=p(j,2);
    end

end

ws=rs/xs;

piteration=piteration+1;

if ws<=10^(-3)

    break

end

end

% COMPUTE LIP DEFORMATION

c=0.5/N;
d=0.5/M;
         for i=1:N
            for j=1:M

                 zz=s(j,i);

            for k=1:N
             for l=1:M
                xi=dx*(i-1);
                yi=dy*(j-1);
                xk=dx*(k-1);
                yl=dy*(l-1);
```

```
I(l,k)=(LD*((yi-yl)-d)*log((((xi-xk)-c)+(LD^2*((yi-yl)-d)^2+((xi-xk)-
c)^2)^(1/2))/(((xi-xk)+c)+(LD^2*((yi-yl)-d)^2+((xi-
xk)+c)^2)^(1/2)))+LD*((yi-yl)+d)*log((((xi-xk)+c)+(LD^2*((yi-
yl)+d)^2+((xi-xk)+c)^2)^(1/2))/(((xi-xk)-c)+(LD^2*((yi-yl)+d)^2+((xi-
xk)-c)^2)^(1/2)))+((xi-xk)+c)*log((LD*((yi-yl)+d)+(LD^2*((yi-
yl)+d)^2+((xi-xk)+c)^2)^(1/2))/(LD*((yi-yl)-d)+(LD^2*((yi-yl)-
d)^2+((xi-xk)+c)^2)^(1/2)))+((xi-xk)-c)*log((LD*((yi-yl)-d)+(LD^2*((yi-
yl)-d)^2+((xi-xk)-c)^2)^(1/2))/(LD*((yi-yl)+d)+(LD^2*((yi-
yl)+d)^2+((xi-xk)-c)^2)^(1/2))));

                I(l,k);
            end

        end
                def=p.*I;

                deft=reshape(def,1,[]);

                defl=sum(deft);

   s(j,i)=zz+RFd*(DEFACTOR*defl-zz);

       xss=xss+abs(s(j,i));

       rss=rss+abs(s(j,i)-sold(j,i));

    end
end

 for j=1:M;
    for i=1:N;
         Hi(j,i)=Hi(j,i)+s(j,i)-sold(j,i);

         Hreal(j,i)=Hreal(j,i)+s(j,i)-sold(j,i);
    end

 end

wss=rss/xss;

iterationnumber=iterationnumber+1;

if wss<=10^(-3)

    break
end
end
```

```
iterationnumber
piteration

% COMPUTE FLOW

j=M;
 for i=1:N;

DPY(j,i)=(H(j,i)^3)*(-25*p(j,i)+48*p(j-1,i)-36*p(j-2,i)+16*p(j-3,i)-
3*p(j-4,i))/(12*dx);
        leak(j,i)=DPY(j,i);

            %simpson rule

     if i==1

         s1=leak(j,i);

     elseif (rem(i+1,2)==0)&&(i>1)

         st1(j,i)=4*leak(j,i);

     elseif (rem(i,2)==0)&&(i<N)

         sc1(j,i)=2*leak(j,i);
     else

         sN=leak(j,i);
     end
  end

st2=reshape(st1,1,[]);
st=sum(st2);

sc2=reshape(sc1,1,[]);
sc=sum(sc2);

Q=10/LD*(s1+st+sc+sN)*dx/3;
Q
figure
mesh(H)
figure
mesh(p)
figure
mesh(s)
```